SHUMAN ZHANG

MASTER OF SCIENCE THESIS

THE ENVIRONMENTAL TOXIN, CHLORPYRIFOS DISRUPTS

MITOCHONDRIAL FUNCTION IN BROWN ADIPOSE TISSUE AND PROMOTES

THE DEVELOPMENT OF OBESITY AND METABOLIC DYSFUNCTION IN MICE

By SHUMAN ZHANG

A Thesis Submitted to the School of Graduate Studies in Partial Fulfillment of the

Requirements for the Degree Master of Science

McMaster University © Copyright by Shuman Zhang, June 2019

i

MASTER OF SCIENCE (2019)

Department of Medical Sciences: Nutrition & Metabolism

McMaster University, Hamilton, Ontario, Canada

Title:	The environmental toxin, chlorpyrifos disrupts mitochondrial function in brown adipose tissue and promotes the development of obesity and metabolic dysfunction in mice
Author:	Shuman Zhang, B.Sc
Supervisor:	Dr. Gregory R. Steinberg, Ph.D.

Number of pages: 81

Abstract:

Chlorpyrifos, one of the most utilized organophosphate pesticides worldwide, is commonly found on many fruits and vegetables, and has been associated with the development of obesity. Brown adipose tissue (BAT) has an abundance of multilocular lipid droplets and mitochondria that express uncoupling protein-1, a protein which generates a futile cycle that contributes to resting energy expenditure in rodents and humans. Reductions in BAT activity are associated with the development of obesity and related metabolic comorbidities including insulin resistance and non-alcoholic fatty liver disease (NAFLD). In this thesis, chlorpyrifos, at a dose which mimics non-occupational exposure, was fed to mice in combination with a control low fat or a high-fat diet and mice were maintained at either room temperature or at thermoneutrality. On a control diet chlorpyrifos had minimal effects on obesity and glucose homeostasis but when combined with a high-fat diet it was found to promote obesity, non-alcoholic liver disease and insulin resistance; effect was more prominent at thermoneutrality. This effect of chlorpyrifos in high-fat diet fed mice was associated with reduced expression of uncoupling protein-1, and disruption of mitochondrial homeostasis within brown adipose tissue, an effect associated with reductions in AMPK and markers of mitophagy. These data suggest that chlorpyrifos may promote obesity and metabolic dysfunction by suppressing brown adipose tissue mitochondrial function.

ACKNOWLEDGEMENTS

The completion of this thesis would not be possible without the support I have received throughout my two years at McMaster University. I am very grateful to everyone who has helped me along the way.

Thank you to my supervisor, Dr. Gregory Steinberg. Thank you for giving me the opportunity to work in this amazing lab. Your advice always pushed me to think a step further and allowed me to develop my own ideas on different subject matters.

Thank you to my committee members, Dr. Katherine Morrison and Dr. Alison Holloway. Thank you for all the support and constructive advice pertaining to my research.

Thank you to my mentor, Dr. Bo Wang. Thank you for guiding and helping me tremendously with my research. It was a great honor to work with you side by side for the past year and a half.

Thank you to all the members of Steinberg Lab. Thank you for the support both in science and in life. It was always fun to come in to the lab and see your smiling faces. You are colleagues, but most important of all, you are amazing friends.

Last but not least, I would like to thank my family and friends. Thank you for the support you have always provided me, both emotionally and physically. You are great pillars of strength and I would not be where I am today without you.

Thank you all.

TABLE OF CONTENTS

LIST OF FIGURES AND TABLES

List of figures

CHAPTER IV - FIGURES

List of tables

CHAPTER II - METHODS AND MATERIALS

LIST OF ABBREVIATIONS

BMI - body mass index

T2D - type 2 diabetes

CVD - cardiovascular disease

NAFLD - non-alcoholic fatty liver disease

CPF - chlorpyrifos

EU - European Union

EPA - Environmental Protection Agency

PND - postnatal day

BAT - brown adipose tissue

WAT - white adipose tissue

UCP1 - uncoupling protein 1

HFD - high-fat diet

CD - control diet

TN - thermoneutral

PKA - cAMP-dependent protein kinase A

AMPK - AMP-activated protein kinase

β3-AR - β3-adrenergic receptor

AC - adenylyl cyclase

PKA - protein kinase A

ATGL- adipose triglyceride lipase

HSL - hormone-sensitive lipase

FFA - free fatty-acid

TCA cycle - tricarboxylic acid cycle

ETC - electron transport chain

H+ - hydrogen ions

ULK1 - unc-51 like autophagy activating kinase 1

LC3 - light chain 3

AMP - adenosine monophosphate

ADP - adenosine diphosphate

RT - room temperature

GTT - glucose-tolerance test

ITT - insulin-tolerance test

AUC - area under the curve

H&E - haemotoxylin-eosin

ORO- oil-red-o

ALT - alanine transaminase

AST - aspartate transaminase

iWAT - inguinal white adipose tissues

eWAT - epididymal white adipose tissues

mtDNA - mitochondrial DNA

PF- pair-feeding

BuCHE - plasma butyrylcholinesterase

TCPy - 3,5,6-trichlorpyridinol

CHAPTER I - INTRODUCTION

1. <u>Obesity and metabolic diseases</u>

Over the past decade, obesity, type 2 diabetes (T2D), cardiovascular disease (CVD) and non-alcoholic fatty liver disease (NAFLD) have become worldwide epidemics. Overweight (body mass index (BMI) 25–29.9 kg/m^2) and obesity (BMI $\geq$30 kg/m^2) are defined by excess accumulation of adipose tissue leading to the impairment of physical and psychosocial health [1]. According to the World Health Organization, the prevalence of obesity has nearly tripled since 1975. In 2016, more than 1.9 billion adults were overweight. Of these, over 650 million were obese [2]. In North America, the situation is even worse: over one-third of adults in the United States are overweight and a similar proportion are obese, while in Canada over one-third are overweight and one-quarter are obese [3]. Such trends are also seen in children with nearly 1 in 7 children and youth in Canada being obese [4].

Not only is obesity itself a health detriment, numerous comorbidities, rooting from excess accumulation of lipid, also pose many health risks including the development of T2D [5], CVD [6] and NAFLD [7]. The development of T2D with obesity is characterized by the combination of peripheral insulin resistance and insufficient insulin production from pancreatic β-cells [8, 9]. CVD mostly refers to the damage to heart or blood vessels caused by atherosclerosis, a buildup of fatty plaques in arteries. Plaque buildup thickens and stiffens arterial walls, which can inhibit blood flow to organs and tissues [10]. NAFLD encompasses a spectrum of chronic liver diseases, characterized by excessive hepatic fat accumulation (steatosis) in the absence of significant alcohol consumption [11]. NAFLD patients have increased risk of liver-

related as well as cardiovascular related mortality [7]. The factors causing T2D, NAFLD and CVD are intertwined with the development of obesity, leading to a vicious cycle. Although these conditions are prevalent in adults, overweight children and adolescents are also at risk for T2D, CVD and NAFLD [12]. Collectively, this presents a dramatic burden to health care systems globally.

In Canada, the annual direct healthcare cost of obesity, including physician, hospitalization and medication costs, is now estimated to be between $5 billion and $7 billion. This annual direct healthcare cost is projected to rise to $9 billion by 2021 [13]. Similarly, the Canadian Diabetes Cost Model has predicted that, nationally, diabetes and its related comorbidities will cost the Canadian health care system $16.9 billion by 2020 [14].

However, in regard to this trend, commonly studied risk factors such as a sedentary lifestyle and high-calorie diets are not enough on their own to explain the global increase of obesity and related diseases. Hence, other risk factors should be explored.

One of the environmental exposures that has been linked to obesity and T2D is the use of synthetic organic chemicals [15-18]. Studies have shed light on the risks brought by exposure to organic pollutants such as pesticides and related chemicals [19, 20]. The wide use of pesticides has increased agricultural productivity, but they have also affected human health. Previous studies have related general pesticide exposure [21, 22] and, more specifically, organophosphate pesticide exposure [23, 24] to a higher incidence of T2D. Therefore, the effect of environmental pollutants and toxins on metabolism is

3

important to investigate.

2. Pesticides and metabolic dysfunction

1.2.1 Chlorpyrifos use and human exposure

Chlorpyrifos (CPF) is one of the world's most utilized organophosphate pesticides in both agricultural and non-agricultural settings and is used extensively because of its effectiveness and efficiency [25]. It is used on corn, tree nuts, soybeans, citrus fruits and over a dozen of other agricultural products. It was first introduced into the marketplace in 1965 and has been widely used globally since then as an insecticide to control crop pests in agriculture, reduce household pests, reduce insect damage on lawns and golf courses, and for mosquito control.

However, accumulating evidence suggests that the use of CPF may negatively affect the function of the central and peripheral nervous systems as well as the reproductive system. Residential use of CPF was eliminated in the United States in 2001 and is being phased out in the European Union (EU) as well [26].

In 2006, Dow AgroSciences, the major manufacturer of CPF in the United States and the EU, began a global phase-out of non-agricultural use of CPF [26]. On August 9th, 2018, the U.S. Ninth Circuit Court of Appeals ordered the Environmental Protection Agency (EPA) to ban CPF within 60 days. The following month, the Department of Justice asked the Ninth Circuit to reconsider its opinion. Although actions have been taken by governments, more research is still needed to demonstrate the effect of such

environmental toxin on human body and to determine if its usage brings more harm than benefits.

Though CPF typically degrades rapidly in the environment, its residues can last for long periods of time [26]. CPF and its metabolite —chlorpyrifos-oxon mediate their effects via the potent inhibition of the enzyme acetylcholinesterase, which is responsible for terminating neurotransmission at cholinergic synapses. Therefore, the primary effect of CPF toxicity is overstimulation of the synaptic system [26]. Moreover, it is worth noting that CPF is extremely lipophilic. In a detailed study of the tissue distribution of CPF, partition coefficients between various tissues and blood were calculated as follows: brain 33:1, liver: 22:1, kidney 10:1, fat 435:1[27]. The accumulation of CPF over time in these organs chronically may lead to pathophysiological change and potential non-reversible functional damage.

There are many exposure pathways for CPF such as ingestion, inhalation and dermal. In the past, inhalation has been a major source for non-occupational exposure to CPF because of its use in residential areas. However, after the US and the EU ban on residential use, dietary exposures to trace levels of CPF on food products became the main source of non-occupational exposure [26] and are more chronic than environmental exposure [28]. Biomonitoring data suggests that average daily exposure to CPF for U.S. adults and children has been estimated to range from 3-24 ng/kg body weight [29].

1.2.2 Existing studies about CPF on metabolism

There are many studies which have investigated the effect of CPF on aspects

other than the central nervous system. Many studies have tried to determine its effect on metabolism and brain function using rodent models, however, they have rarely looked into the mechanism(s) by which such effects were occurring.

A previous study done by Lassiter et al. [30] has shown that rats gain excess weight after developmental exposure to CPF. In this study, time-pregnant rats were dosed daily by gavage with CPF (2.5 mg/kg body weight) from gestational day 7 through the end of lactation on postnatal day (PND) 21(PND 0 as the day the rat was born), and offspring were weighed regularly from birth until young adulthood (PND 95-101). The CPF exposure caused excess weight gain in males beginning at PND 45 and reaching levels 10.5% above control by PND 72, while volumetric measurements showed that the exposed males were also 12% larger than controls. This data suggests that the exposure of CPF may cause delayed disturbances in body weight and body density.

Another study, done by Kondakala et al. [31] showed that CPF exposure can lead to non-cholinergic effect such as decreased hepatic carboxylesterase activity and decreased hepatic hydrolysis in a high-fat diet dependent manner. In this study, male C57BL/6J mice were fed a normal or high-fat diet for 4 weeks and administered a single dose of vehicle or CPF (2.0 mg/kg; oral gavage).

Studies were also done to explain the relationship between CPF and microbiota. A study done by Liang et al. [32] showed that CPF disrupts the structural integrity of the gut barrier, leading to increased lipopolysaccharide entry into the body and low-grade inflammation. Moreover, mice given CPF-altered microbiota also gained more fat and had lower insulin sensitivity.

While the effects of many of these organic chemicals and environmental toxins on food intake and lipid metabolism, especially adipogenesis, have been studied intensely [33], relatively little is known about the potential role of environmental toxicants in regulating resting energy expenditure, a critical component of energy balance.

Though many studies were done using animal models, there is no study done with human subjects. The toxic nature of CPF makes it unethical to expose human with such substance in any dosage. Observational studies are also hard to be conducted because the amount of pesticides in different food and the amount of food people consume vary dramatically from subject to subject.

3. Adipose tissue

1.3.1 Adipose tissue types

There are three types of adipose tissues in mammals: brown adipose tissue (BAT), white adipose tissue (WAT) and brite, for brown-in-white, or beige adipose tissue. BAT is unique to mammals and is mainly activated by cold exposure to maintain body thermostasis [34]. It has an abundance of multilocular lipid droplets and mitochondria, which contains iron and gives it the "brown" color; while WAT stores large amounts of lipid in unilocular droplets and is low in mitochondria. BAT dissipates energy in the form of heat through uncoupling protein 1 (UCP1) which is found in the mitochondrial inner membrane [34]. WAT can also recruit UCP1-positive cells and this induces the differentiation of beige adipocytes through a process called "browning" [35]. These beige

7

adipocytes have been shown to have similar molecular characteristics as BAT [36]. BAT and beige adipose tissue have a higher metabolic capacity than WAT [37] and therefore may be very important organs for regulating resting energy expenditure.

Previously, scientists had believed that BAT only existed in infants but not in adolescents or adults. However, in 2007, Nedergaard et al. [38] showed that some adults exhibited BAT activity and that activated BAT could contribute to resting energy expenditure. Since then, more studies have acknowledged the contribution of active BAT to metabolism in humans among various population and environments [39-42]. While the extent of this contribution is widely debated and highly variable between studies, a consistent finding is that adults with obesity have reduced BAT thermogenesis both basally and in response to cold temperatures [39,42,43]. Therefore, it is worthwhile to study BAT and its regulation to potentially combat obesity and other metabolic diseases.

1.3.2 BAT function and regulation

Human BAT is defined by its elevated expression of UCP1 [44]. When mice are housed at room temperature (21-22 degree Celsius) the genetic deletion of *Ucp1* has no effect on the development of high-fat diet (HFD) induced obesity or insulin resistance [97]. However, surprisingly, when *Ucp1* null mice are housed under thermoneutral conditions (TN, 28-29 degree Celsius) and fed a HFD they develop greater obesity and insulin resistance [45]. The explanation for this finding is that, in contrast to humans, room temperature elicits a chronic thermal stress to mice [95], which leads to increases in UCP1 dependent and independent thermogenesis (e.g. shivering) and elevations in food

8

intake in order to defend body temperature [96]. However, in a thermoneutral environment, where thermal stress is eliminated and therefore there is no need for shivering or non-shivering thermogenesis, the primary role of UCP1 is for diet-induced thermogenesis, similar to humans (Insert Mueez Cell metabolism reference). Therefore, thermoneutral housing in mice more precisely models the role of BAT/UCP1 in similar to humans who also live in a thermoneutral environment because of the existence of clothing and heating.

The expression of *Ucp1* in BAT is controlled by a thermogenic gene program of transcription factors, co-activators and protein kinases including PGC1α, PRDM16, cAMP-dependent protein kinase A (PKA), p38 MAP kinase and AMP-activated protein kinase (AMPK) [46-48]. And all of these reactions and regulations require normal mitochondrial function.

Acutely, BAT activation is regulated by the brain, which receives signals regarding ambient temperature (i.e. cold) and nutritional status (i.e. food intake). This leads to activation of the sympathetic nervous system, which stimulates the release of norepinephrine. Norepinephrine binding to the β3-adrenergic receptor (β3-AR) stimulates the activation of adenylyl cyclase (AC), subsequently leading to an increase of cAMP and the activity of protein kinase A (PKA). PKA activates lipolytic enzymes such as adipose triglyceride lipase (ATGL) and hormone-sensitive lipase (HSL) which leads to the release of free fatty acids (FFA), which are transported to mitochondria through the carnitine shuttle system to be used as substrates in beta-oxidation. Beta-oxidation, also called fatty-acid oxidation, produces acetyl-coA, which then enters the tricarboxylic

9

acid cycle (TCA cycle). Reducing equivalents, NADH and FADH$_2$, produced by beta-oxidation and the TCA cycle enter the electron transport chain (ETC) where hydrogen ions (H$^+$) are transported from the mitochondrial matrix to the intermembrane space, generating an electrochemical proton gradient. There are two ways that these hydrogen ions can go back to the mitochondrial matrix. These hydrogen ions can be transported from the mitochondrial intermembrane space by ATP synthase, which generates ATP when H+ pass through. However, when UCP1 is present, H+ are able to re-enter the mitochondrial matrix without ATP synthase or generating ATP. Thus, UCP1 dissipates the proton motive force through a proton leak across the inner mitochondrial membrane [49], which in turn increases flux through beta-oxidation and the TCA cycle resulting in the generation of heat.

4. <u>Mitochondrial Homeostasis and the Role of AMPK</u>

1.4.1 Mitochondrial Homeostasis

BAT activity is mainly regulated through UCP1 and β3-adrenergic receptor stimulation [50], which induces downstream transcription of genes involved in mitochondria biogenesis [51]. BAT relies heavily on mitochondrial respiration to maintain its normal physiological function. Therefore, mitochondrial dysfunction is an important component in the pathophysiology of various metabolic and cardiovascular diseases [52].

Mitochondrial biogenesis and mitophagy are two pathways that regulate mitochondrial content and are important for preserving homeostasis. Mitophagy, literally meaning "mitochondria autophagy", is the process of intracellular degradation to promote the clearance of damaged mitochondria and maintain "healthy mitochondria" in the cells [53]. Removal of damaged mitochondria through autophagy requires two steps: induction of general autophagy and priming of damaged mitochondria for selective autophagic recognition [54]. It is highly controlled and regulated by various activators and inhibitors; among them AMPK is an upstream regulator which can affect many different pathways downstream.

1.4.2 The Role of AMPK in mitophagy

AMPK has been shown to mediate the degradation of mitochondria through mitophagy [55, 56]. It directly phosphorylates the unc-51 like autophagy activating kinase 1 (ULK1) at several residues including the S555 site. The activation of ULK1 signals to form mature phagophores, which are necessary to capture cytosolic contents and deliver them to the lysosome [57]. Microtubule-associated protein light chain 3 (LC3) is also involved, which undergoes processing and lipidation from LC3 I to LC3 II to become active. LC3 is responsible for the elongation of the double-membrane vesicle, which changes from a phagophore to an autophagosome when the membrane has completely encapsulated the constituents [58].

AMPK can be activated by physiological, hormonal, and nutritional stimulus. Such stimuli trigger the increase of the adenosine monophosphate/ adenosine

diphosphate to ATP ([AMP]/[ADP]: [ATP] ratio) [59]. Previous study done by Mottillo et al. [60] showed that □3-adrenergic stimuli (e.g. cold, norepinephrine) increased AMPK activity in brown and white fat and mice lacking functional AMPK had defects in BAT mitochondrial content and reduced browning of white fat. Such defects made mice intolerant of cold or reduced their ability to increase fatty acid oxidation in response to a high-fat diet. These defects in mitochondrial function were associated with decreased markers of mitophagy including the phosphorylation of ULK1^{S555} and LC3B-II expression.

Interestingly, recent studies by Andrea Llanos (an MSc student working in Drs. Holloway and Steinberg laboratories) have identified that the pesticide CPF decreases *Ucp1* expression and mitochondrial respiration *in vitro*. Immortalized BAT cells derived from UCP-1 luciferase reporter mice, or wild-type FVB/N mice were used in experiments. Specifically, she found that when these immortalized BAT cells were treated with CPF at 1pM, 1nM, and 1µM doses, there were reductions in *Ucp1* promoter activity, mRNA and protein levels by greater than 25%. In further analysis, including whole cell respiration assays and mitochondrial enzyme activity assays, CPF reduced the expression of *Cox8b*, *Cox2*, and *Pgc1α*, genes important for mitochondrial function, while also reduced maximal respiratory capacity and the activity of cytochrome c oxidase, complex IV of the ETC. These data demonstrate that CPF directly suppresses UCP-1 expression and BAT function at concentrations as low as 1pM.

5. <u>Hypothesis</u>

My hypothesis is that exposure of C57BL6/J mice to CPF in the diet will suppress UCP1 expression and brown adipose tissue function resulting in greater development of obesity, NAFLD and insulin resistance.

CHAPTER II - METHODS AND MATERIALS

2.1 Animal experiments

All experiments were approved by the McMaster University Animal Ethics Committee and conducted under the Canadian guidelines for animal research (AUP # 16-12-41). All mice used in this study were 7-week-old C57BL6/J males (purchased from Jackson Laboratory, ME, USA). All groups were weight matched and randomized to treatments at the beginning of each experiment. The researchers were not blinded to the experimental groups during the experiment and testing. Mice were housed in pathogen–free microisolator cages and located in a room on a 12-h light-dark cycle with lights on at 7:00 a.m. As thermal stress is an important determinant regulating energy expenditure and obesity [61], mice were housed at either room temperature (RT, 21-23℃), or a thermoneutral temperature (TN, 29-30℃) more akin to the condition in which humans reside [62]. Each cage had two mice.

CPF is detected in a wide range of foods including fruits, vegetables, grains, beans, nuts, legumes, dairy, meat, fish and eggs [63]. Hence, we added CPF (Toronto Research Chemicals, C425300, ON) to the diet instead of gavage to mimic the exposure for humans. The mice were fed with a control diet (CD, 10 kcal% fat; D12450H Research Diet; New Brunswick, NJ) or a high-fat diet (HFD, 45 kcal% fat; D12451 Research Diet) and regular tap water *ad libitum* for 14 weeks. To avoid acetylcholinesterase inhibition [64] and mimic the level of environmental CPF exposure, the low dose CPF diet was supplemented with 2 mg per kg diet (/kg DT) CPF for the first week; 3 mg/kg DT diet CPF for the second and third weeks and 5 mg/kg DT CPF for 11 weeks, to provide 0.5 mg/kg BW (per kg body weight) CPF. Gradually increasing doses

at the beginning of the treatment allowed mice to avoid any potential acute physiological response to CPF. High dose CPF was 4 times higher than the low dose. The doses of CPF used in this study were selected as they were below the dose known to induce neurotoxicity.

For both CD and HFD cohorts, grouping and dosing were as below:

1) CD/HFD with TN environment;

2) CD/HFD with 0.5 mg/kg BW CPF with TN environment (low dose);

3) CD/HFD with 2 mg/kg BW CPF with TN environment (high dose);

4) CD/HFD with RT environment;

5) CD/HFD with 0.5 mg/kg BW CPF with RT environment (low dose);

6) CD/HFD with 2 mg/kg BW CPF with RT environment (high dose);

No signs of cholinergic toxicity were observed in mice during the experiment as food intake and activities were normal. Body weight (per mouse, n = 10) and food intake (per cage, n = 5) were measured weekly.

2.2 Metabolic measurements

Body composition was monitored weekly by a Bruker's minispec Whole Body Composition Analyzer. Respiration rate was measured using the Comprehensive Laboratory Animal Monitoring System (CLAMS, Columbus Instruments, Ohio, USA) after 11 weeks of treatment. Animals were housed in separate chambers, with *ad libitum* tap water and milled HFD or CD for five days. Measurements for food intake, oxygen

consumption (VO2), carbon dioxide production (VCO2), and heat (kcal/hr) were averaged per day.

Glucose-tolerance test (GTT) and insulin-tolerance test (ITT) were performed after 12 and 13 weeks of treatment, respectively. Mice were fasted for 6 h. Then they were intraperitoneally injected with glucose (1 g/kg in saline) or insulin (0.7 U/kg for CD mice and 1 U/kg for HFD mice). Blood samples were collected by tail bleeding and analyzed with glucometer (Accu-chek, Roche, 04680448003) immediately before and at 20, 40, 60, 90 and 120 min after an intraperitoneal injection of glucose or insulin. Area under the curve (AUC) was calculated.

2.3 Histology

Histological samples harvested from mice were initially fixed in 10% neutral buffered formalin for 12h at 4 °C, washed with 70% ethanol 3 times, and embedded in paraffin and sectioned (5 µm thickness). Following deparaffinization, samples were subsequently processed and stained with haemotoxylin-eosin (H&E) by the Department of Pathology and Molecular Medicine at the McMaster University Children's Hospital. Images were taken using a Nikon 90i Eclipse (Nikon Inc., NY, USA) upright microscope at a magnification of 4X. For each slide which contained 3 or 4 samples, 10 photos were taken and representative photos are showed in the results section.

For immunostaining, sections were heated in citrate buffer for 20 min, blocked with 5% goat serum in TBS containing 0.3% Triton X-100 for 2 h, then incubated sequentially with primary antibodies overnight and secondary antibody for 1 h. The color

was developed using a VECTOR® NovaREDTM Peroxidase (HRP) Substrate Kit (#SK-4800, Vector Laboratories). Sections were then mounted with a mounting medium (Vector Laboratories, Burlingame, CA). Images were taken using a Nikon 90i Eclipse (Nikon Inc., NY, USA) upright microscope at a magnification of 4X. For each slide which contained 3 or 4 samples, 10 photos were taken, and representative photos are showed in the results section.

For liver used for oil-red-o (ORO) lipid staining, tissues were infiltrated with 30% sucrose for 24h after formalin fixation, then embed with OTC and frozen in isopentane cooled in liquid nitrogen. Cryo-sections of 10-um-thick were rinsed with PBS, then stained with ORO [65] for 10 min, washed with 60% isopropanol for 3 times then mounted with an fluoromount aqueous mounting medium (Sigma Life Science, Lot #SLBH7382V). Images were taken using a Nikon 90i Eclipse (Nikon Inc., NY, USA) upright microscope at a magnification of 4X and 10X. For each slide which contained 3 or 4 samples, 10 photos were taken, and representative photos are showed in the results section.

2.4 Transmission Electron microscopy (TEM)

BAT (interscapular) was fixed in 2% glutaraldehyde (2% v/v) in 0.1 M sodium cacodylate buffer (pH 7.4) for at least 24 hours. Thin sections were cut on a Leica UCT ultramicrotome and picked up onto Cu grids. Sections were post-stained with uranyl acetate and lead citrate. The preparation, fixation, and sectioning were performed by the electron microscopy group at McMaster University Medical Center.

Electron micrographs shown in the results section were obtained with an AMT 4-megapixel CCD camera (Advanced Microscopy Techniques, Woburn, MA) mounted in a JEOL JEM 1200 EX TEMSCAN transmission electron microscope (JEOL, Peabody, MA, USA) operating at an accelerating voltage of 80 kV.

To perform the quantification, 25 images per sample were acquired by random sampling. Each group had 3-4 samples. Mitochondria with disrupted cristae and total mitochondria were counted from each image, averaged per sample, and then expressed as % cristae disruption (mitochondria with disrupted cristae over total mitochondria). Criteria for dysmorphic mitochondria with disrupted cristae included any observable disorganization, vacuolization, or dissolution of cristae within mitochondria [66]. Mitochondria diameter was measured by the shortest diagonal in each mitochondrion in each photo using Image J software (National Institutes of Health, Bethesday, USA) and graphed as %frequency of different diameter length.

2.5 Western Blot

Lysate preparation

Tissues were chipped in approximately 30 or 50 mg pieces, for BAT and liver tissues, respectively, on dry ice. Each piece was weighed and placed in cryotubes chilled on ice. The amount of cell lysis buffer added to each sample equals to weight (in mg)*20 µL of cell lysis buffer for BAT and weight (in mg)*10 µL of buffer (50 mM HEPES pH 7.4, 150 mM NaCl, 100 mM NaF, 10 Na-pyrophosphate, 5 EDTA mM , 250 mM sucrose, 1 mM DTT, and 1 mM Na-orthovanadate, 1% Triton X, and Complete protease inhibitor

cocktail (Roche)) for liver. Two ceramic beads were placed in each cryotube, and a Precellys 24 homogenizer (Bertin Technologies, Paris, France) was set to shake 2 x 20 seconds at 5500 rpm. Lysates were then centrifuged at 13 000 x rpm for ten minutes at 4 °C to separate protein from other remnants. The protein fraction was collected and transferred to a 1.5 mL eppendorf chilled on ice. The process of centrifugation and transfer were repeated one more time to ensure that there is no lipid in the protein extraction. Lysates were then immediately used or stored at -80 °C.

Sample preparation

To determine the concentration of protein within the lysate sample, the Pierce BCA protein assay kit (Thermo Fisher Scientific, MA, USA) was used. Lysates were diluted 1:20 in ultrapure H_2O (Milli-Q) and standards were provided in the kit. BAT samples were then prepared to a final concentration of 1 µg protein/µL lysate and liver samples to a final concentration of 2 µg protein/µL lysate using SBJ cell lysis buffer and 4x SDS sample buffer (40% glycerol, 240 mM, Tris-HCl pH 6.8, 8 % SDS, 0.04 % bromophenol blue, 5 % β-mercaptoethanol, with a 1:50 dilution of 1M DTT). All samples were boiled at 95 °C for 5 mins before used in Western blotting.

SDS-PAGE, transfer, and blocking

SDS polyacrylamide gels were prepared the day prior to running gel electrophoresis and were stored in dampened paper towels at 4 °C overnight. 7.5, 10, or 12 % gels were made, depending on the size of the protein being blotted for. If running

multiple proteins vary greatly in size in one gel, a gel could also be made with 10% for the upper half and 12% for the lower half. For each run, β-tubulin or β-actin was used as a loading control for total protein blots. Electrophoresis was run at 90 V through the stacking gel and 110 V through the separating gel at room temperature. Separated proteins were transferred onto nitrocellulose membranes electrically at 90 V for 120 mins using wet transfer techniques. Subsequently, membranes were rinsed in 1 x Tris-buffered saline (TBS, 50 mM Tris, 150 mM NaCl, 1 M HCl, pH 7.4) for 5 mins then blocked in 5 % bovine serum albumin (BSA) in 1 x TBS with 0.1 % tween-20 (TBST) for 1 hour at room temperature.

Antibody incubation, immunodetection, and densitometry

Membranes were cut and incubated in primary antibody (see Table 1) with 5 % BSA in 1 x TBST at 4 °C on a rocker overnight. On the next day, membranes were washed with 1 x TBST for 5 min and incubated with appropriate secondary antibody (see Table 1) in 5 % BSA in TBST for 1 hour on a rocker at room temperature. After 3 x 5 mins wash in 1 x TBST, proteins of interest were imaged using electrochemiluminescence. Densitometry was performed using Image J software (National Institutes of Health, Bethesday, USA). All phospho/total proteins were converted to ratios and expressed as relative to control, meanwhile other proteins were normalized to β-tubulin/β-actin and expressed as relative to control.

Table 1 – Antibodies used for Western blot

Primary Antibody	Company (Product J Dilution	Secondary Antibody	Dilution
pACCS79	CST (3661)	1:1000	Rabbit	1:10000
ACC	CST (3662)	1:1000	IgG HRP- linked	
pAMPKαT172	CST (2535)	1:1000	CST (7074)	
AMPKα	CST (2532)	1:1000		
UCP1	ADI (UCP11-A)	1:1000		
pULK1S555	CST (5869)	1:1000		
ULK1	CST (8054)	1:1000		
p62	CST (5114)	1:1000		
LC3B	CST (2775)	1:1000		
β-tubulin	Invitrogen (32-2600)	1:5000	Mouse; IgG HRP- linked CST (7076)	

2.6 RNA Isolation & Real-time quantitative polymerase chain reaction (RT-qPCR)

Chipped tissues were lysed in 1 mL TRIzol reagent (Invitrogen, CA, USA) on ice. Two ceramic beads were placed in each cryotube, and a Precellys 24 homogenizer (Bertin Technologies, Paris, France) was set to shake 2 x 20 seconds at 5500 rpm. Samples were then incubated at room temperature for 5 mins and were centrifuged for 10 mins at 13 000 x g at 4 °C. 200 μL chloroform was added and shaken vigorously before allowing the samples to incubate at room temperature for another 2 mins. The samples were centrifuged again for 10 mins at 13 000 x g at 4 °C before collecting the supernatant.

An equal amount of 70 % ethanol was added to the tube containing the supernatant and vortexed. In order to extract and purify RNA, we used the RNeasy kit (Qiagen, CA, USA). During the elution step, 15ul of RNase-free water was used for each time and this step was repeated for one more time to make sure all RNA was captured. A NanoPhotometer (MBI, QC, Canada) was used to determine the concentration (ng/µL) and purity (260/280, 260/230) of the extracted RNA. RNA was immediately diluted using RNase-free water to a concentration of 2 µg/13.5 µL, and was then used to synthesize cDNA by dNTPs and random hexamers for 5 mins at 65 °C and cooled to 4 °C, then SuperScript III, First Strand Buffer, and DTT for 5 mins at 25 °C, 60 mins at 50 °C, 15 mins at 70 °C, and cooled to 4 °C (Invitrogen, CA, USA). Synthesized cDNA was either immediately used or stored at - 80°C.

Using an optimized mastermix including 1.7 µL RNase-free water, 1 µL 10X Buffer, 1 µL $MgCl_2$ (25 mM), 1 µL dNTPs (2 mM), 0.05 µL Ampli-Taq Gold, and 0.25 µL TaqMan probe per reaction, RT-qPCR was performed with a 10 µL reaction (5 µL diluted cDNA, 5 µL mastermix) in a qPCR thermocycler (Corbett Rotor Gene 6000, MBI, QC, Canada). Within the thermocycler, the samples were incubated at 95 °C for 10 mins to activate the Ampli-Taq Gold, and were amplified with 40 cycles of 10 secs at 95 °C and 45 secs at 60 °C. Slopes were corrected for and thresholds were set at 0.05 using the Corbett Rotorgene software (Corbett Research, Australia). All PCR products and TaqMan probes (see Table 2) were purchased from Invitrogen (CA, USA).

Relative gene expression was calculated using the comparative Ct ($2^{-\Delta Ct}$) method, where values were normalized to a housekeeping gene (*Ppia*) and expressed as

relative to control (control group in each diet or housing condition).

Table 2- TaqMan probes purchased from Invitrogen (CA, USA)

Gene	TaqMan Assay ID N°
Cidea	Mm00432554_m1
Cox8b	Mm00432648_m1
Pgc1α	Mm00440939_m1
Ppia	Mm02342430_g1
Ucp1	Mm01244861_m1
Prdm16	Mm00712556_m1

2.7 Triglyceride assay: Liver and Serum

About 50 mg of tissue was homogenized in chloroform: methanol (2:1) and a portion of the organic phase was freeze-dried down and resuspended in isopropanol. Serum or tissue samples were assayed for triglyceride amount using a Triglyceride Colorimetric Assay Kit (Cayman Chemical, MI).

2.8 Mitochondrial DNA (mtDNA)

About 20 mg of BAT were incubated with tail lysis buffer (100mM Trois-Cl, 5mM EDTA, 200mM NaCl, 0.2%(w/v) SDS, 100µg/ml proteinase K) at 37 degree Celsius overnight. The next day, centrifuge the lysate at 13000 rpm for 20 mins. Transfer the supernatant and add 500µl 100% isopropanol. Invert tubes to precipitate DNA and centrifuge at 13000 rpm at room temperature for 15 mins. Decant isopropanol and add

700 µl 75% ethanol and then centrifuge at 13000 rpm for 10 mins again. Remove the ethanol and let the tubes air dry. Resuspend DNA in 20 µl MilliQ water at 55 degree Celsius for 20 mins. Real-time PCR were run as previously described. Long-mtDNA-F (# 207405385, Integrated DNA Technologies, IA, USA), long-mtDNA-R (#207405386), short-mtDNA-F (#207405387) and short-mtDNA-R (#207405388) were used as probes in the reaction.

2.9 Non-Esterified Fatty Acid Assay

Blood was collected via retro-orbital sinus (endpoint) and placed in eppendorf tubes chilled on ice. Plasmas were isolated by centrifugation set at 4 °C and spun at 8000 rpm for 10 minutes. The supernatant was collected, and stored at -80 °C. MaxDiscovery non-esterified fatty acids (NEFA) Assay Kit (Bioo Scientific, TX, USA) was used to measure the level of serum free fatty-acid.

2.10 Serum ALT and AST

Blood was collected as described in the previous section. MaxDiscovery alanine transaminase (ALT) enzymatic assay kit and MaxDiscovery aspartate transminase (AST) enzymatic assay kit (Bioo Scientific, TX, USA) were used to measure the serum level of ALT and AST.

CHAPTER III --RESULTS

3.1 Chlorpyrifos exacerbates HFD induced obesity, glucose intolerance and insulin resistance in a HFD dependent manner

On a control diet, CPF supplementation showed no influence on body weight (**Figure 1A and 1B**), fat mass (**Figure 1C and 1D**), whether at room temperature or at thermoneutrality. When fed with the high-fat diet, mice treated with CPF had higher body mass at both room temperature (**Figure 2A**) and thermoneutrality (**Figure 2B**). This increase in body mass was associated with greater fat mass when housed at thermoneutrality **(Figure 2C and 2D)**.

On a control diet, CPF supplementation had no influence on glucose tolerance (**Figure 3A and 3B**) or insulin sensitivity (**Figure 3C and 3D**). However, consistent with increases in adiposity when fed a high-fat diet, CPF treatment led to impaired glucose tolerance (**Figure 4A and 4B**) and insulin sensitivity (**Figure 4C and 4D**).

These data indicate that CPF exacerbates the development of obesity, glucose intolerance and insulin resistance in a high-fat diet dependent manner.

3.2 Chlorpyrifos promotes adipocyte hypertrophy and liver injury

Consistent with the increased body mass and adiposity in HFD-CPF treated mice, CPF increased the size of lipid droplets in both inguinal white adipose tissues (iWAT) (**Figure 5A**) and epididymal white adipose tissues (eWAT) (**Figure 5B**). Such adipocyte hypertrophy was aggravated with the dose of CPF, in conjunction with use of HFD, at both room temperature and thermoneutrality. HFD-TN mice treated with CPF also had elevated circulating free fatty acids and circulating triglycerides (**Figure 5C, 5D**).

Obesity, insulin resistance and elevated free fatty acids are associated with NAFLD [68]; therefore, we analyzed the livers of mice. HFD-TN mice treated with CPF had higher liver weight (**Figure 6A**) and more liver triglyceride (TG) (**Figure 6B**). Oil red O and H&E staining showed bigger lipid droplets in the liver of CPF treated mice (**Figure 6C**). Serum biomarkers of liver damage alanine aminotransferase (ALT) and aspartate aminotransferase (AST) [69] were also elevated with CPF treatment (**Figure 6D and 6E**).

These data indicate that CPF promotes adipocyte hypertrophy and NAFLD in mice.

3.3 Chlorpyrifos reduces UCP1 expression in brown adipose tissue

Obesity is associated with reduced BAT activity [72]. To specifically examine the metabolic capacity of BAT we injected mice with a □3-agonist known to specifically activate UCP1-mediated thermogenesis [44] and found that in mice treated with CPF, oxygen consumption was reduced. This suggests that reduced energy expenditure with CPF treatment may be due to defects in BAT thermogenesis.

To examine the mechanisms contributing to obesity we examined energy intake and expenditure using metabolic cages. CPF supplementation in HFD reduced basal (**Figure 7A**) oxygen consumption at thermoneutrality in the CLAMS metabolic testing, but not at RT (**Figure 7B**). This reduction in oxygen consumption of thermoneutral mice was independent of physical activity which was not altered by CPF **(Figure 7C)**. CPF

also increased food consumption at both room temperature and thermoneutrality (**Figure 7D and 7E**) which may have also contributed to the increased weight gain.

To investigate whether a reduction in BAT thermogenesis was accompanied with alterations in histology we performed H&E staining and found that chronic CPF treatment caused whitening of the BAT at both room temperature and thermoneutrality when the mice were fed with HFD (**Figure 8A**) but not with CD (**Figure 8B**). Consistent with the increase in lipid content in BAT of HFD-fed mice, there was reduced expression of *Ucp1* in high-fat diet fed mice (**Figure 8C and 8D).** This effect was not observed when mice were fed a control diet (**Figure 8E**). Immunohistochemistry and Western blotting both showed that UCP1 protein was also lower in BAT of CPF treated mice with HFD at both room temperature and thermoneutrality (**Figure 8F and 8G**).

These data indicate that consistent with the development of obesity and metabolic dysfunction, CPF in combination with a HFD, impairs BAT function and the expression of UCP1.

3.4 Chlorpyrifos impaired mitochondria function

In addition to the expression of UCP1, mitochondrial function is vital for maintaining thermogenesis in BAT. Transmission electron microscopy images showed that mice treated with CPF and fed a high-fat diet at thermoneutrality had an increased abundance of large mitochondria and mitochondria with disrupted cristae (**Figure 9A and 9B**). On the contrary, and consistent with other parameters, there was no significant

change in the morphology of mitochondria in mice fed a control diet with CPF (**Figure 9C and 9D**).

Furthermore, we performed PCR on mitochondrial DNA (mtDNA), the short-range PCR reflects total mtDNA content and the long-range PCR amplifies intact mitochondria DNA template because when there is the strand breaks the amplification will stop. Increased short fragment (**Figure 9E**), but not long fragment (**Figure 9F**), indicated the accumulation of damaged mtDNA but not intact mtDNA in the BAT of CPF-treated mice [94].

These data showed that dietary exposure to chlorpyrifos impairs mitochondrial function in brown adipose tissue *in vivo*.

3.5 Chlorpyrifos altered mitochondrial homeostasis by inactivating AMPK

Mitophagy is the mitochondrial-specific process of autophagy that recycles damaged or dysfunctional mitochondria into their cellular constituents in order to maintain a healthy network of mitochondria [73]. To understand the cellular mechanism that was leading to the accumulation of dysfunctional mitochondria in the BAT of mice exposed to CPF, we analyzed signalling pathway related to autophagy, as shown in figure 11. AMPK phosphorylation of ULK1^{S555}, which is required to trigger mitophagy [55] was lower in the BAT of mice treated with CPF (**Figure 10A**). LC3 elongates the double-membrane vesicle, which becomes an autophagosome from a phagophore when the membrane has completely encapsulated the constituents [58]. In alignment with a defect in mitochondrial clearance, the lipidation of the autophagy protein LC3B was

lower **(Figure 10A)**. Greater accumulation of the autophagy adaptor protein p62 **(Figure 10A)** suggested the deficiency in autophagy signalling in the proteasome [74]. The changes with ULK1^{S555}, LC3B-II and p62 are similar to what is found in the brown adipocytes lacking AMPKβ1/β2 subunits [60].
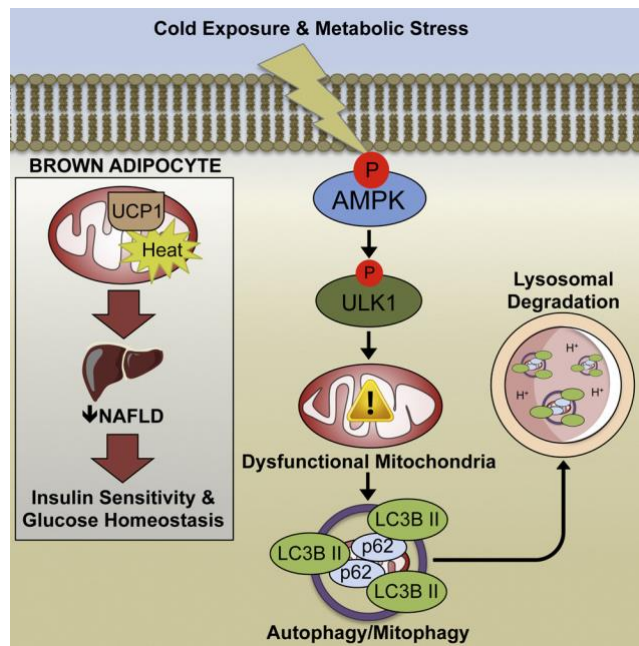

Figure 11. AMPK induction of mitophagy signaling pathway [60]

AMPK phosphorylates ULK1 mostly at site S555. ULK1 is a key signaling enzyme in the activation of mitophagy and induction of phagophore formation. LC3 is necessary for elongating the double membrane vesicle to form autophagosome, when activated by lipidation to become LC3B II. Overaccumulation of autophagy adaptor p62 delays the delivery of proteasomal contents to proteasome.

Phosphorylation of Thr (172) of AMPKα accounts for most of the activation by AMPK [75] and AMPK increases fatty acid oxidation through inhibitory phosphorylation of ACC. ACC is rapidly regulated by reversible phosphorylation which inactivates ACC; thus inhibiting acetyl-coA becoming malonyl-coA to enter fatty acid synthesis and inhibit fatty acid oxidation [76]. Lower pAMPKT172 and pACC were detected in the BAT of CPF treated mice **(Figure 10B)**, suggesting AMPK activation was low and so was the downstream fatty acid beta-oxidation.

These data suggest that CPF reduces brown adipocyte respiration via a mechanism involving reductions in AMPK that may involve impaired mitochondrial homeostasis due to the inhibition of mitophagy and phosphorylation of ACC.

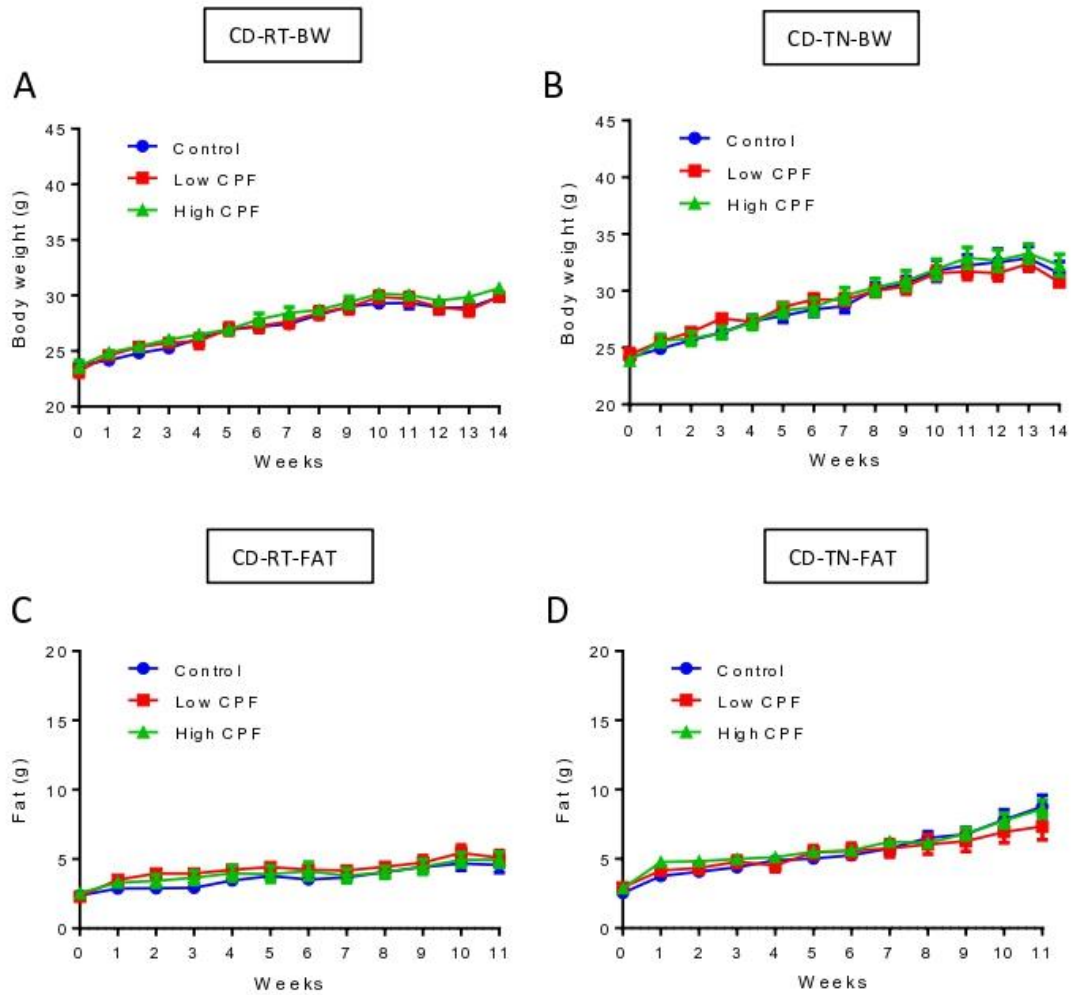**Chapter IV: FIGURES**

Figure 1

Figure 1. CPF has no effect on body weight and adiposity in mice fed a control diet.
C57BL6J male mice were treated with CD (10 kcal% fat) supplemented with two doses of CPF at room temperature (RT) or thermoneutral condition (TN). (A-B) Body weight of mice at RT (A) or TN (B). (C-D) Fat mass of mice at RT (C) or TN (D). Data presented are mean ± SEM, n = 10, * p < 0.05.
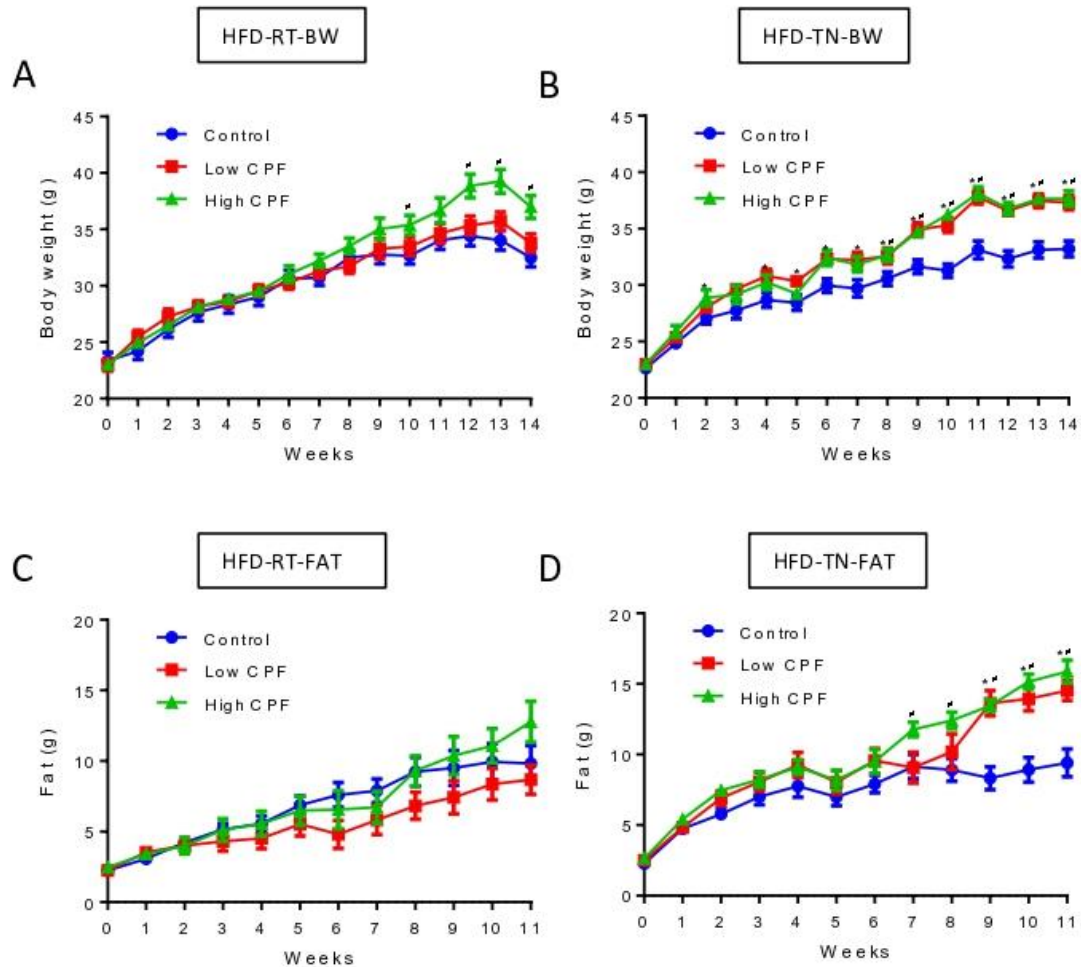
Figure 2

Figure 2. CPF promotes obesity and adiposity in mice fed a high-fat diet.

C57BL6J male mice were treated with HFD (45 kcal% fat) supplemented with two doses

of CPF at room temperature (RT) or thermoneutral condition (TN). (A-B) Body weight

of mice at RT (A) or TN (B). (C-D) Fat mass of mice at RT (C) or TN (D). Data

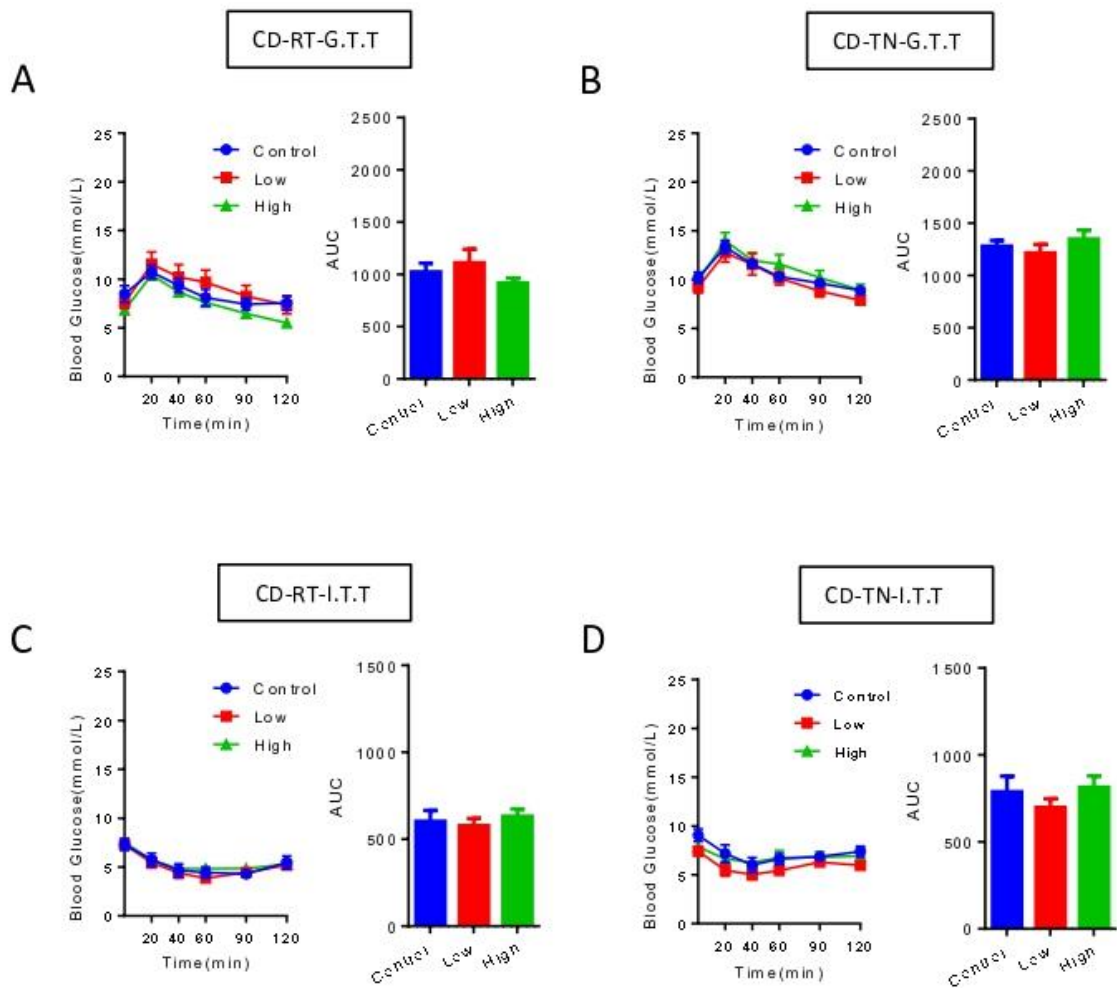presented are mean ± SEM, n = 10, * p < 0.05.

Figure 3. CPF has no effect on glucose tolerance and insulin sensitivity in mice fed a control diet. C57BL6J male mice were treated with CD (10 kcal% fat) supplemented with two doses of CPF at room temperature (RT) or thermoneutral condition (TN). (A-B) Glucose tolerance test (GTT) of mice at RT (A) or TN (B). (C-D) Insulin tolerance test (ITT) of mice at RT (C) or TN (D). Data presented are mean ± SEM, n = 10, * $p < 0.05$.
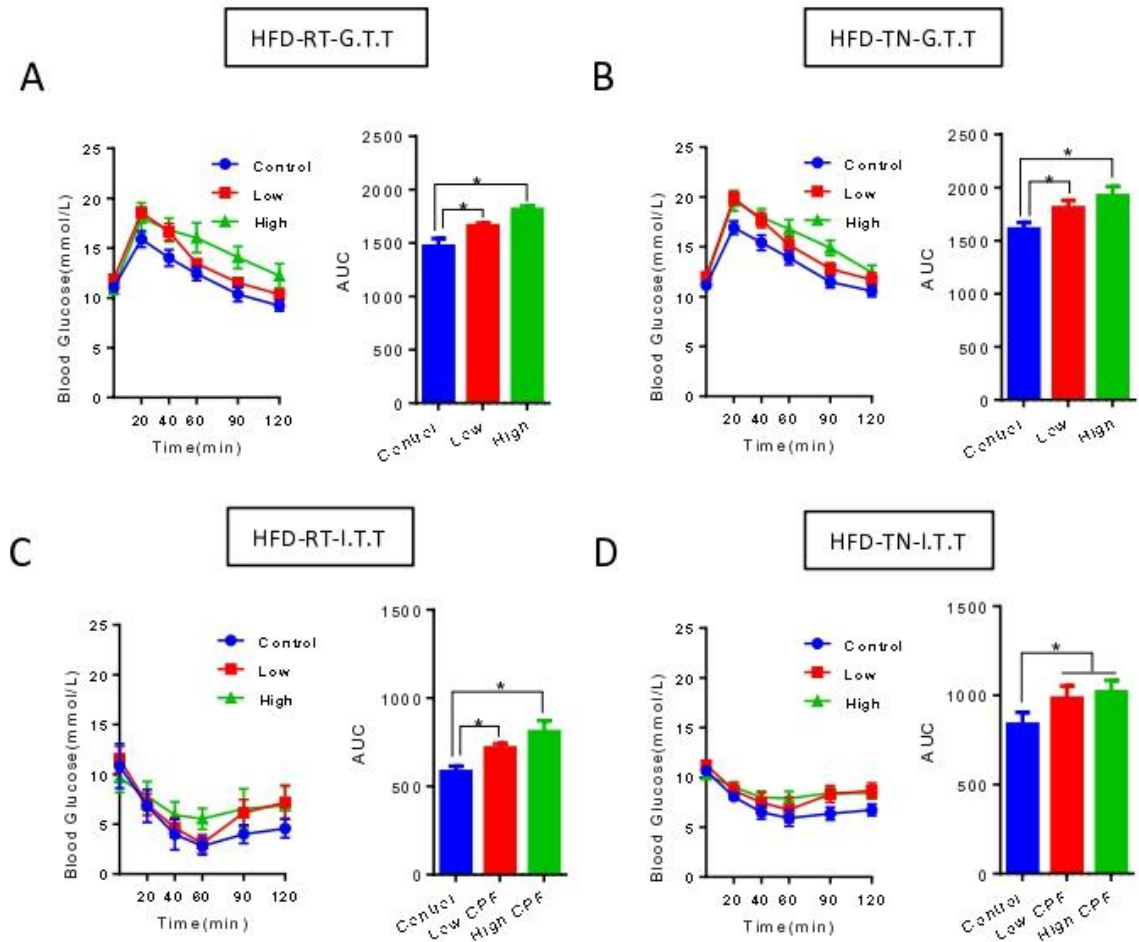
Figure 4. CPF promotes metabolic dysfunction in mice fed a high-fat diet.

C57BL6J male mice were treated with HFD (45 kcal% fat) supplemented with two doses

of CPF at room temperature (RT) or thermoneutral condition (TN). (A-B) Glucose

tolerance test (GTT) of mice at RT (A) or TN (B). (C-D) Insulin tolerance test (ITT) of

mice at RT (C) or TN (D). Data presented are mean ± SEM, n = 10, * p < 0.05.

Figure 5

iWAT H&E Staining

A

HFD-RT

HFD-TN

Control   Low CPF   High CPF

B

eWAT H&E Staining

HFD-RT

HFD-TN

Control   Low CPF   High CPF
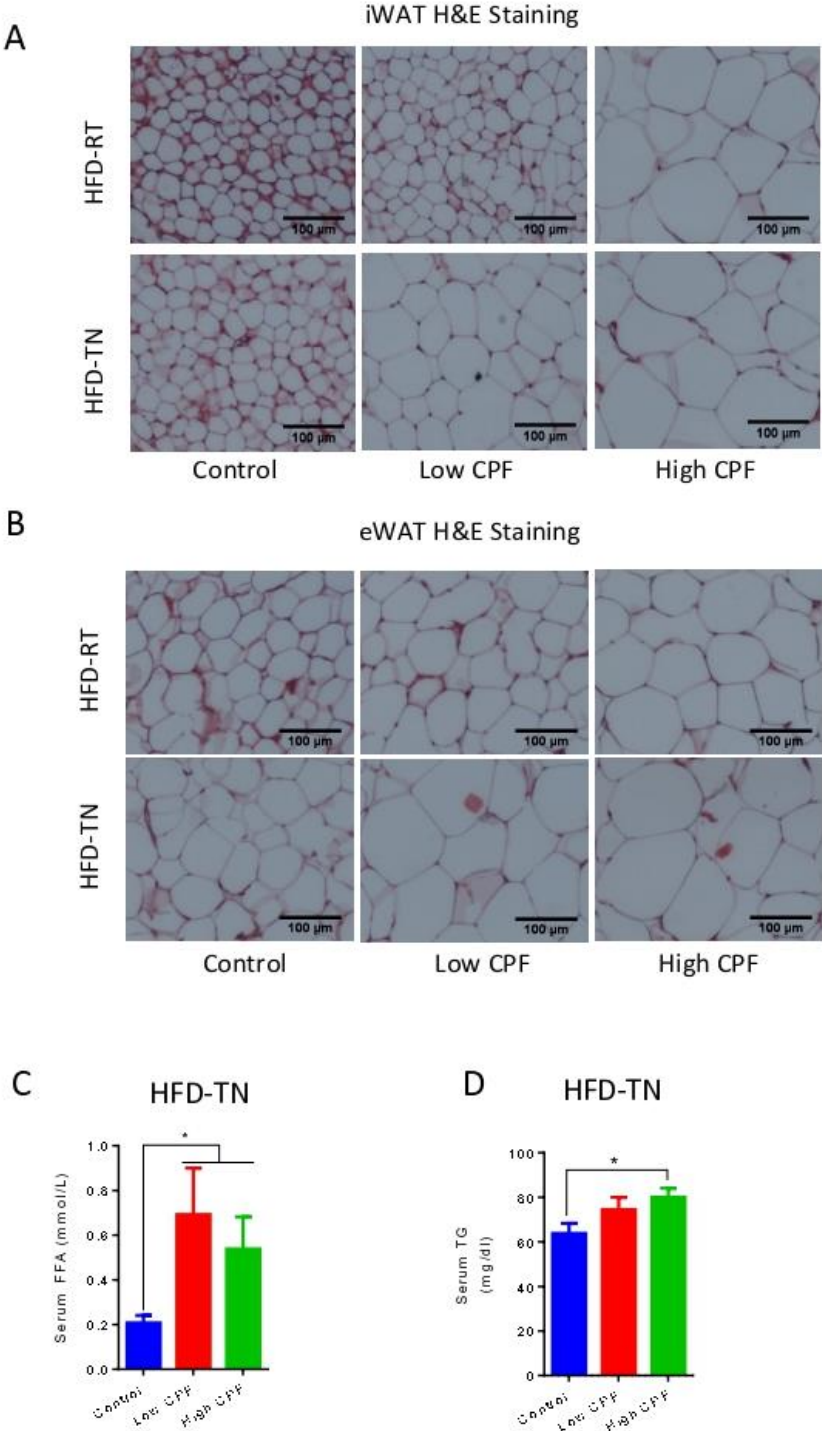
C

HFD-TN

D

HFD-TN

Figure 5. CPF promotes adipocytes hypertrophy and circulating lipid level. C57BL6J male mice were treated with HFD (45 kcal% fat) supplemented with two doses of CPF at room temperature (RT) or thermoneutral condition (TN). (A) Representative images of H&E stained inguinal white adipose tissue (iWAT). (B) Representative images of H&E stained epididymal white adipose tissue (eWAT). (C) Serum free fatty acid (FFA) and triacylglycerol (TG) levels. Data presented are mean ± SEM, n = 10, * $p < 0.05$. Scale bar = 100 μm.

Figure 6

A HFD-TN

B HFD-TN

HFD-TN-Liver

C

Oil Red O

H&E

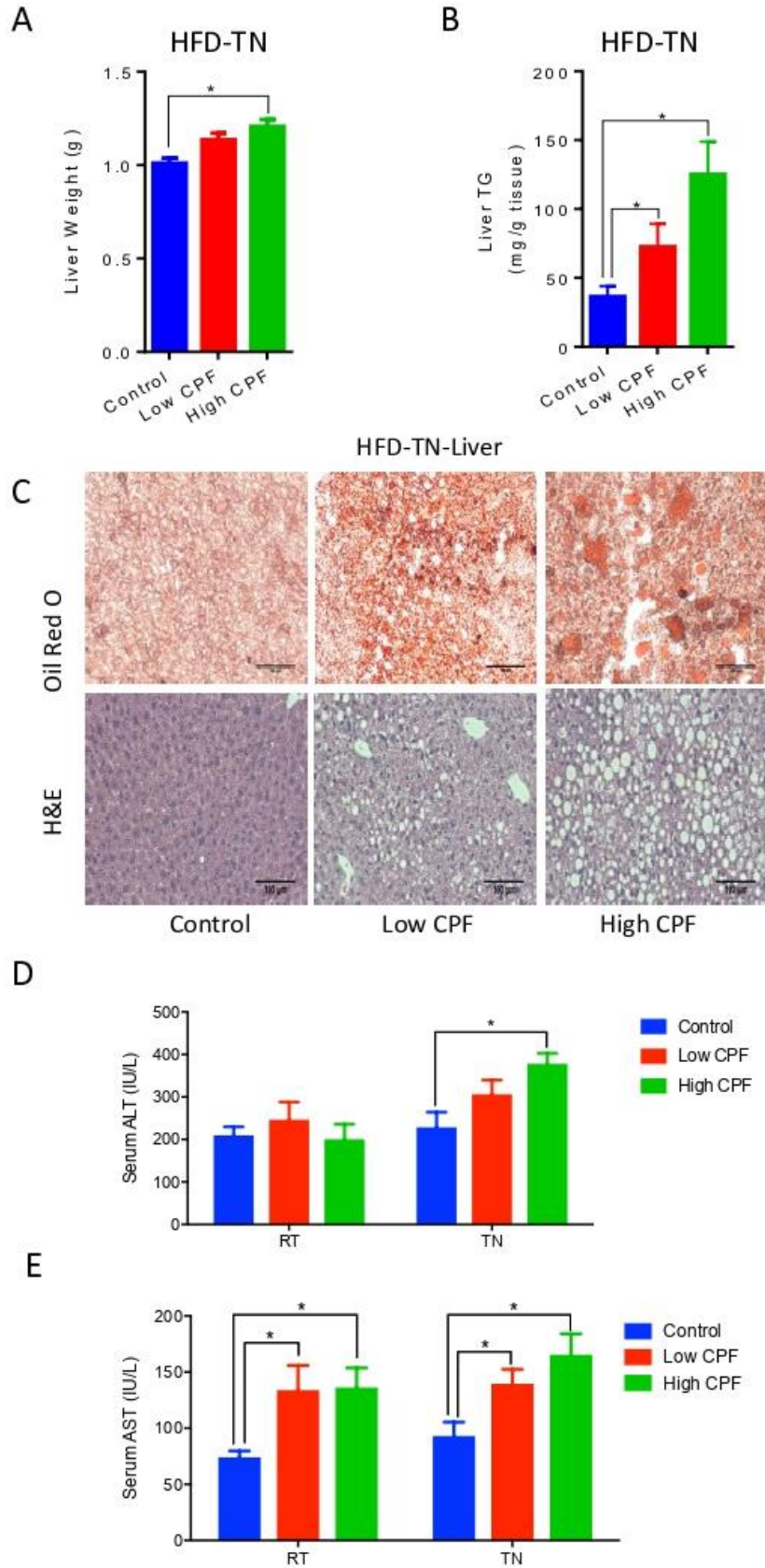Control   Low CPF   High CPF

D

E

Figure 6. Dietary exposure to chlorpyrifos promotes liver injury and NAFLD. C57BL6J male mice were treated with HFD (45 kcal% fat) supplemented with two doses of CPF at room temperature (RT) and thermoneutral condition (TN). (A) Liver weight. (B) Liver TG concentration. (C) Representative images of Oil Red O stained liver lipids. (D) Serum alanine aminotransferase (ALT) and aspartate aminotransferase (AST) levels. Data presented are mean ± SEM, n = 10, * $p < 0.05$. Scale bar = 100 μm.
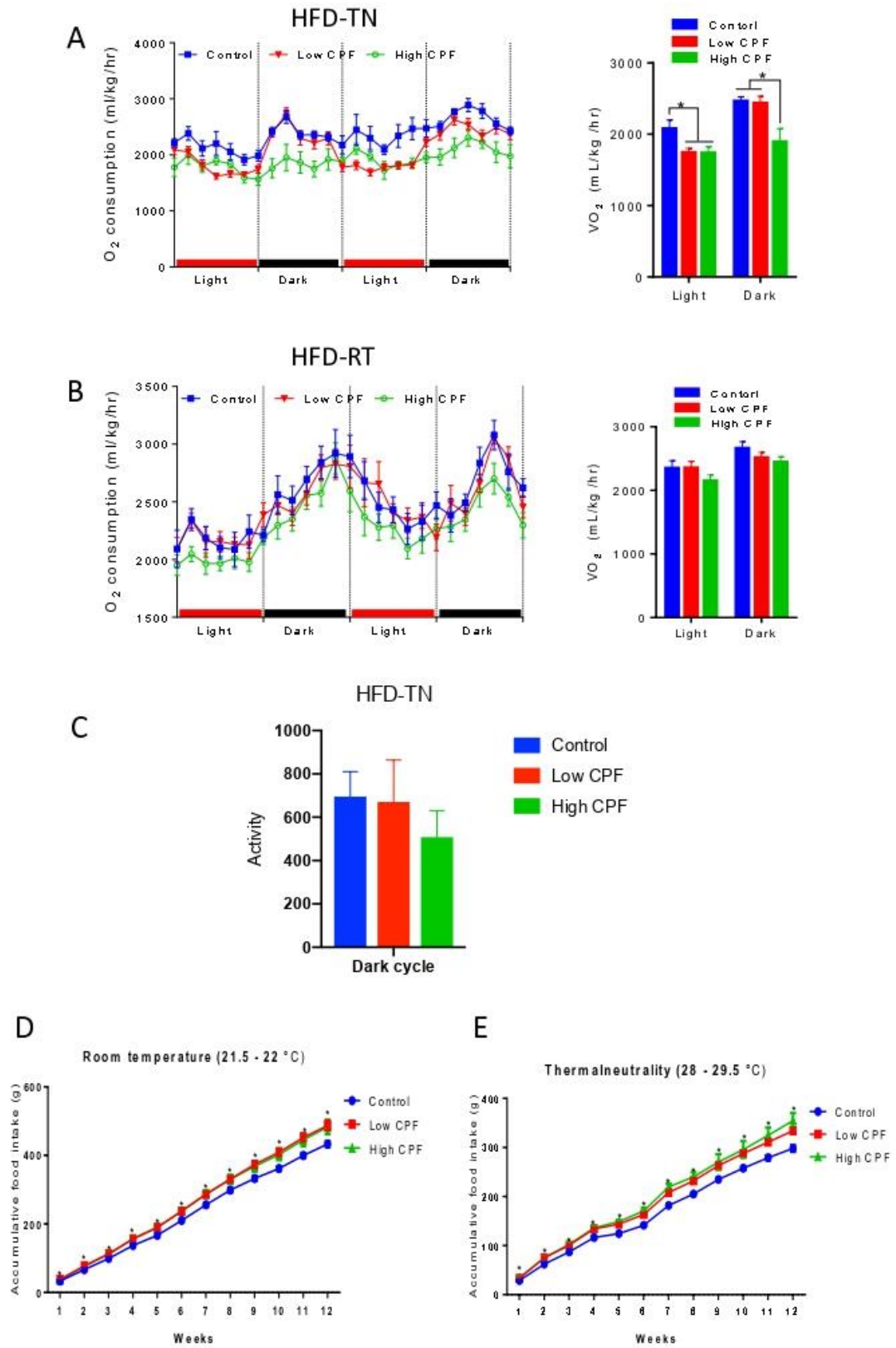
Figure 7

Figure 7. CPF with HFD decreases mice basal metabolic rate. C57BL6J male mice were treated with HFD (45 kcal% fat) supplemented with two doses of CPF at room temperature (RT) or thermoneutral condition (TN). Basal oxygen consumption rate of mice after 10 weeks of treatment at TN (A) or RT (B). Physical activity at TN (C). Accumulative food intake at RT(D) or TN(E). Data presented are mean ± SEM, n = 10, * $p < 0.05$.

Figure 8

A

BAT H&E Staining

HFD-RT

HFD-TN

Control　　　Low CPF　　　High CPF

B

BAT H&E Staining

CD-RT

CD-TN

Control　　　Low CPF　　　High CPF

C

HFD-TN BAT

- Control
- Low CPF
- High CPF

D

HFD-RT BAT

- Control
- Low CPF
- High CPF

Figure 8 cont.

E
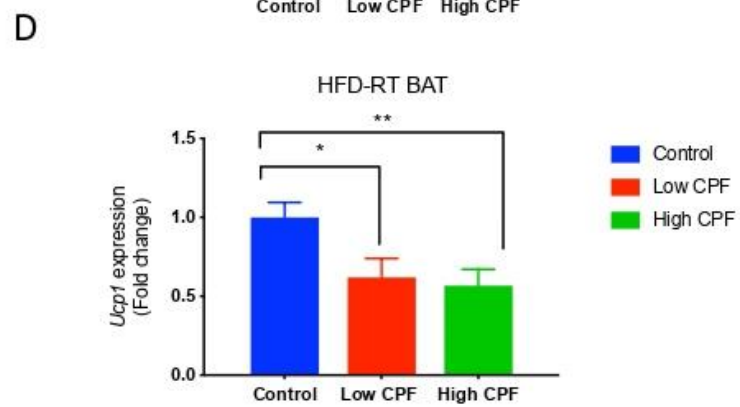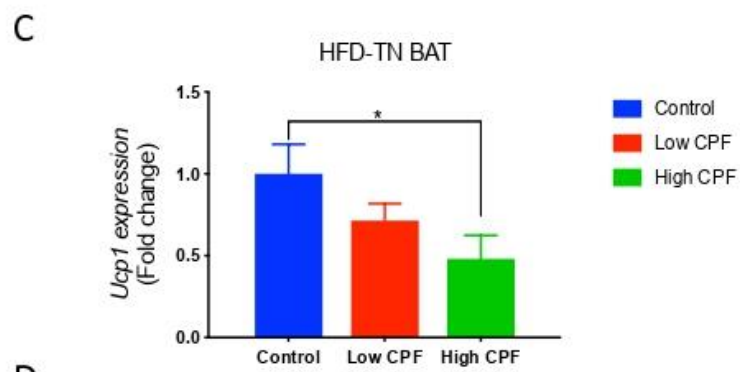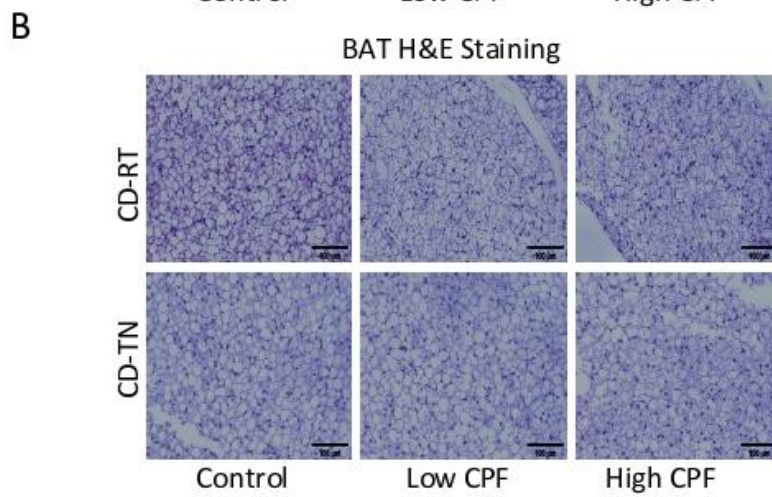
CD-BAT
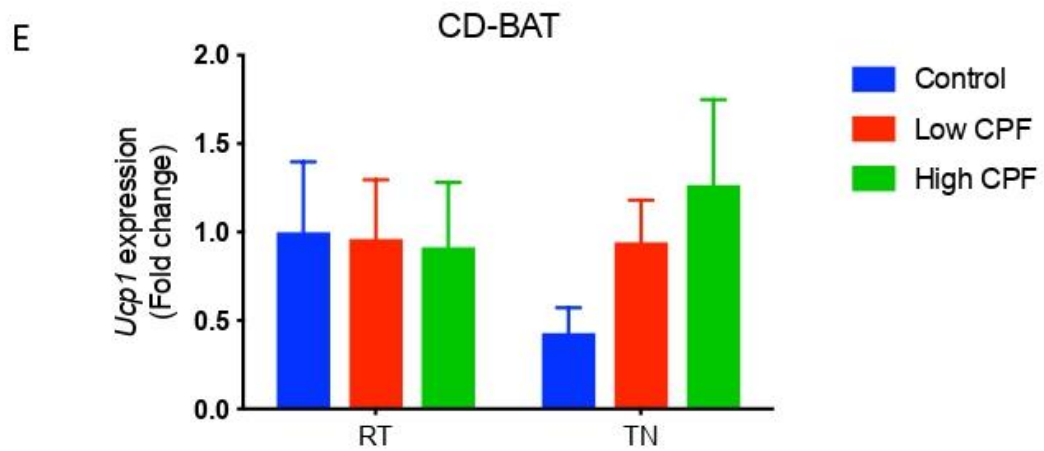
F

BAT-UCP1 Immunohistochemistry
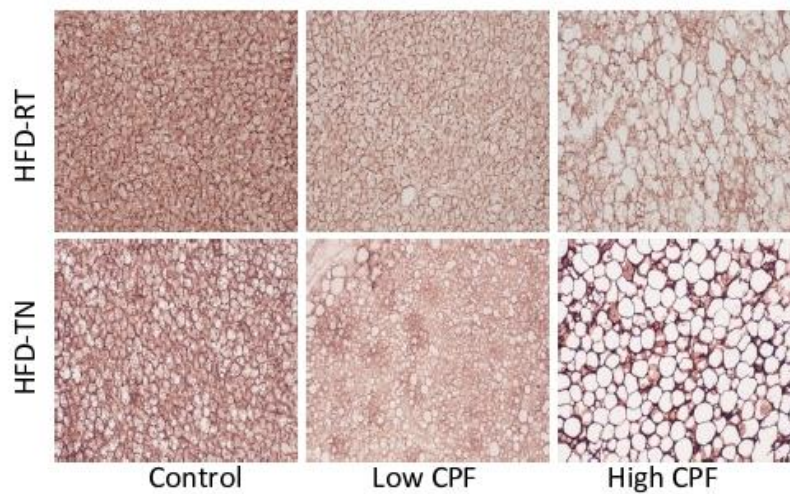
G

BAT-UCP1 Western Blot
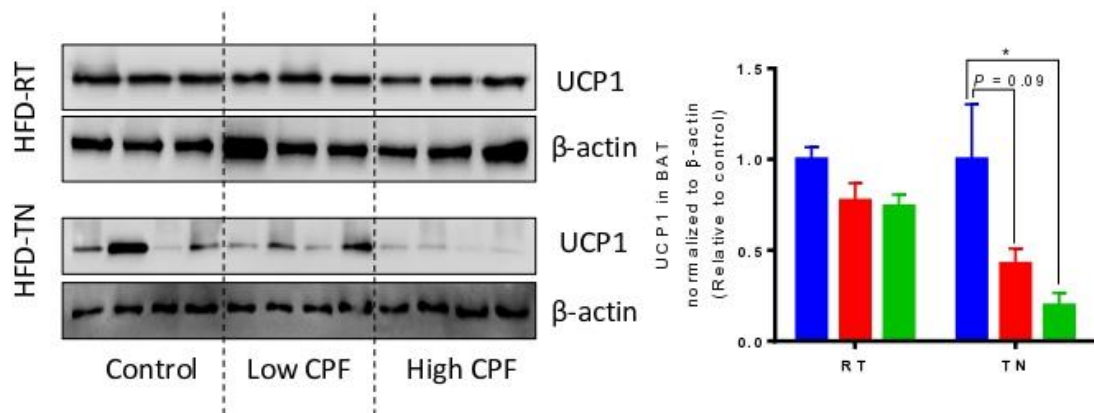
Figure 8. Dietary exposure to chlorpyrifos impairs thermogenesis in brown adipose tissue. C57BL6J male mice were treated with CD (10 kcal% fat) or HFD (45 kcal% fat) supplemented with two doses of CPF at room temperature (RT) or thermoneutral condition (TN). (A-B) Representative images of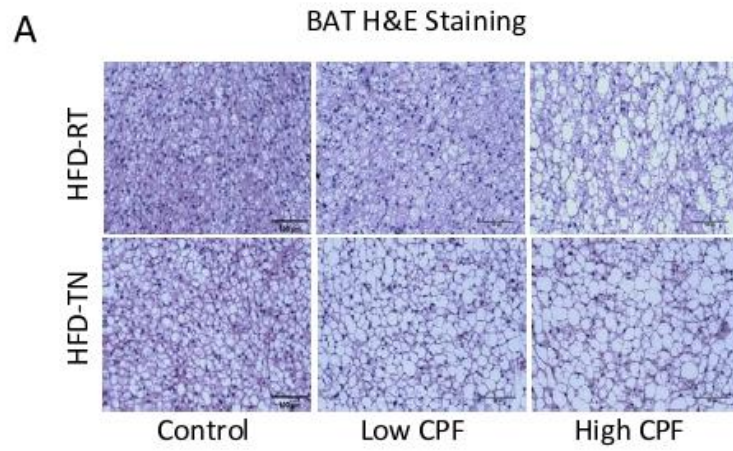 H&E stained brown adipose tissue (BAT) with HFD(A) and CD(B). (C-D) mRNA expression level of brown adipose genes in BAT of mice with HFD at TN (C) and RT (D). (E-F) mRNA expression level of brown adipose genes in BAT of mice with CD at TN (E) and RT (F). (G) Representative immunohistochemistry images showing UCP1 in BAT. (H) UCP1 protein in BAT. Data presented are mean ± SEM, n = 10, * p < 0.05, ** p < 0.01. Scale bar = 100 μm.

Figure 9

A
HFD-TN-BAT mitochondria

Control   CPF

Disrupted cristae (%)

B

Control
High CPF

Frequency (%)

HFD-TN-BAT mitochondria diameter (nm)

C
CD-TN-BAT mitochondria

Control   CPF

D

Control   CPF

Frequency (%)

CD-TN-BAT mitochondria diameter (nm)

E

Control
High CPF

mtDNA normalized to nuDNA

Short fragment

F

Control
High CPF

mtDNA normalized to nuDNA

Long fragment
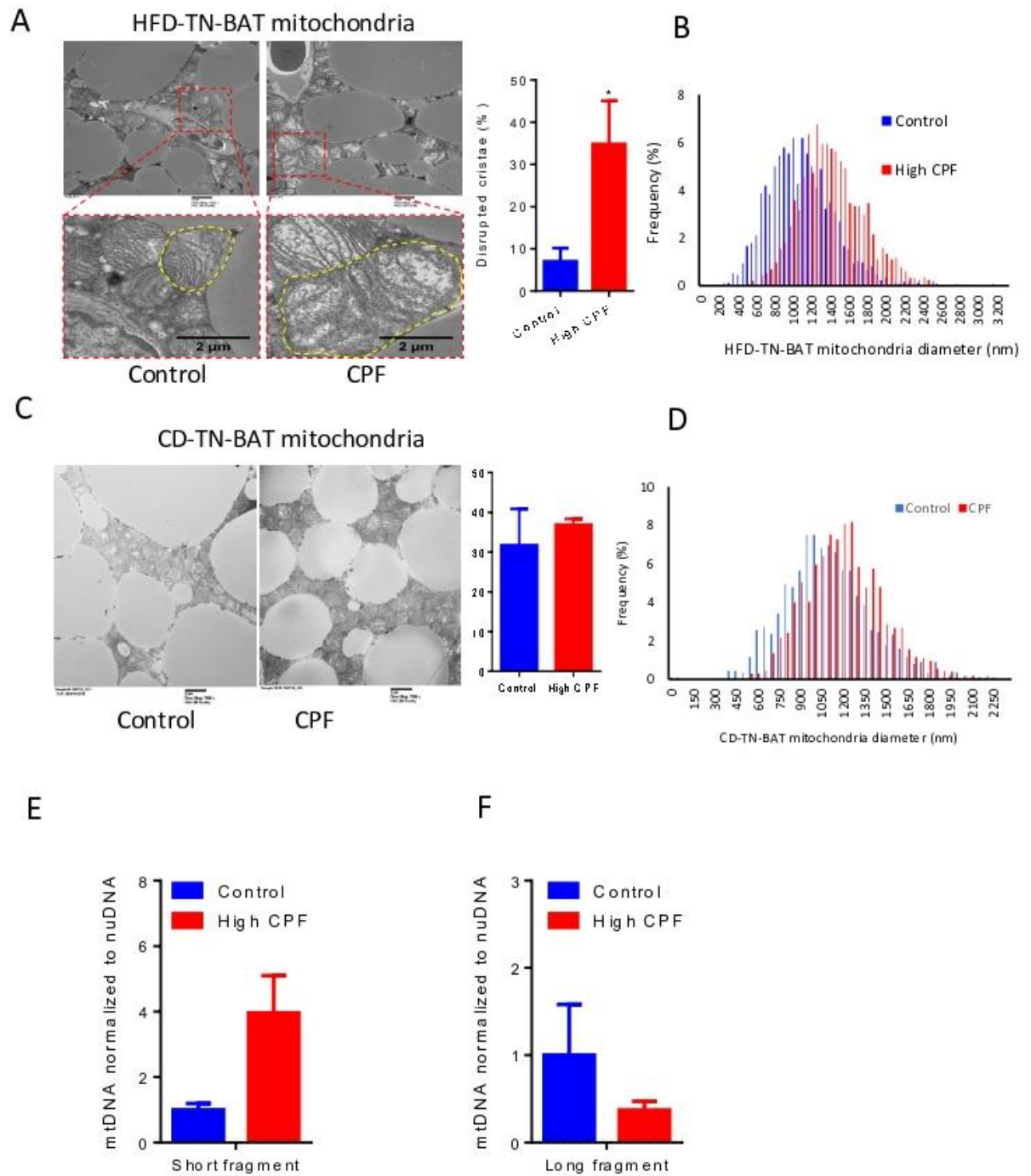
Figure 9. CPF impairs mitochondria homeostasis. C57BL6J male mice were treated with CD (10 kcal% fat) or HFD (45 kcal% fat) supplemented with two doses of CPF at thermoneutral condition (TN). (A) Representative electron micrographs for mitochondria (Left) and quantification of disrupted mitochondria cristae (Right) in BAT of HFD treated mice at TN. (B) Diameter distribution of mitochondria in BAT of HFD treated mice at TN. (C) Representative electron micrographs for mitochondria (Left) and quantification of disrupted mitochondria cristae (Right) in BAT of CD treated mice at TN. (D) Diameter distribution of mitochondria in BAT of CD treated mice at TN. (E) Short fragment of mitochondrial DNA of BAT. (F) Long fragment of mitochondrial DNA of BAT. Data presented are mean ± SEM, n=4 for electron micrographs and n=10 for mtDNA, * $p < 0.05$.

Figure 10

A — HFD-TN BAT

pULK1^555 — ULK1 — p62 — LC3B-II — β-tubulin

Control | Low CPF | High CPF

B — HFD-TN BAT

pACC — ACC — pAMPKaT172 — AMPKa — β-actin
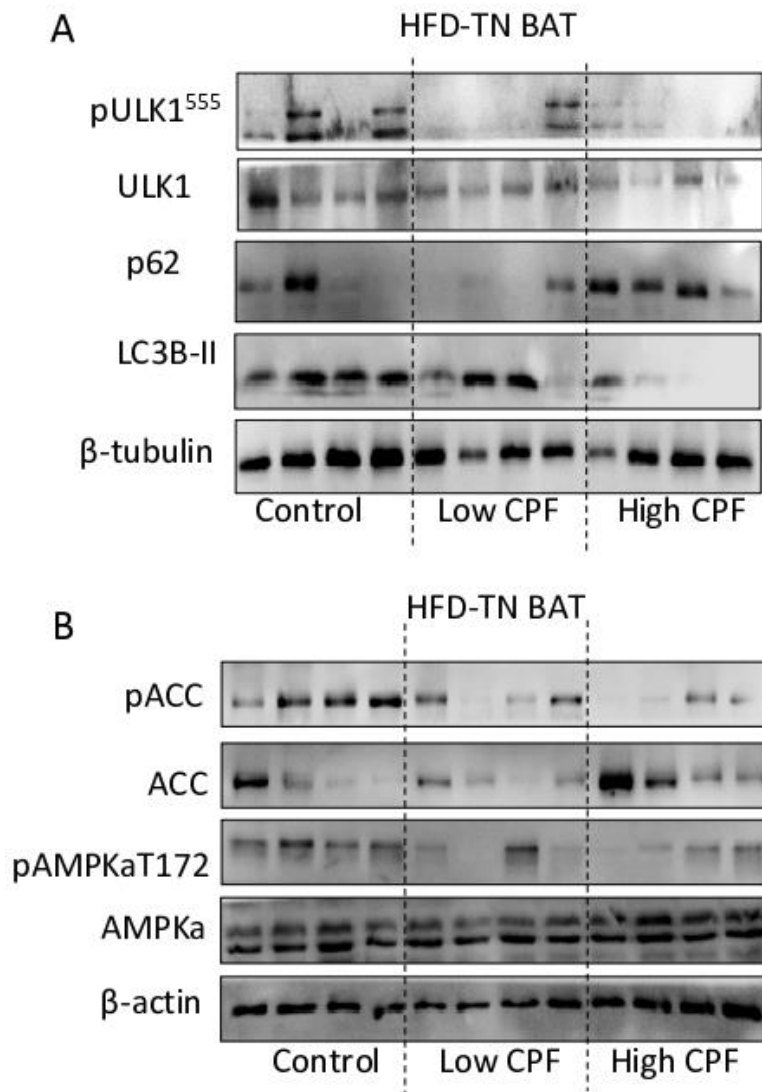
Control | Low CPF | High CPF

Figure 10. CPF impairs mitophagy via AMPK dependent mechanism.

(A-B) Mitophagy (A) and AMPK signaling (B) related proteins in BAT of mice treated with CPF with HFD at TN for 14 weeks.

Chapter V: DISCUSSIONS & FUTURE DIRECTIONS

Due to its lipophilic nature, adipose tissue is the major site of CPF accumulation [77, 78]. Once ingested, it is very unlikely that CPF will be metabolized until lipolysis occurs [77]. However, as this type of accumulation in adipose tissue is non-lethal, less research had been carried out to investigate its effects. In comparison, there is a large amount of studies detailing its damage to the nervous and reproductive systems.

A previous study has shown that chronically, high-dose CPF (30 mg/kg BW) inhibits plasma butyrylcholinesterase (BuCHE) and brain acetylcholinesterase activity, but this effect was not found with low dosages (2.5 mg/kg BW) [79]. To ensure the doses in this study did not cause any damage and mimics daily life, the CPF concentrations are purposely selected to not induce neurotoxicity. However, it is important to note that environmental CPF levels, usually entering the body through regular fruit and vegetable consumption, may also contribute to the overall dosage.

Several studies have shown that CPF alters glucose and lipid metabolism [32, 71, 80-82]; two of them reported that CPF promotes obesity and insulin resistance through the gut microbiome [32,82]. In the study that used a mouse model, the dosing was 5 mg/kg corn oil, which is similar as the low dosage in our study (5 mg/kg diet). However, the direct effect of CPF on adipose tissue's function and pathophysiological change is still unclear. Adipose tissue is mainly used for energy storage and is also an endocrine organ that acts as a regulator of energy homeostasis [35]. Unlike WAT, which is unilocular and stores large amounts of lipid, BAT is abundant in mitochondria and dissipates energy into heat through non-shivering thermogenesis via UCP1 [34]. Due to its nature of consuming energy instead of producing ATP, BAT is a key determining

factor of resting energy expenditure and subsequent total energy balance. Increasing energy expenditure by activating BAT becomes a promising strategy to prevent obesity and its related comorbidities [83]. At these doses of long-term dietary exposure of CPF, it impaired BAT mitochondrial function and promoted obesity in HFD-fed mice.

In addition, CPF also damaged the mitochondria in BAT and decreased its thermogenic capability. In humans, although BAT is present in adults and could be activated after cold exposure [42], people with obesity were less responsive to cold stimulus compared to their lean counterparts [84]. The amount of BAT and its activity also declined with aging in humans [85] and was inversely correlated with body mass index (BMI) [40]. The mechanisms of these changes are still not clear. However, given the widespread usage of CPF in both agricultural and non-agricultural settings, our study would suggest that CPF accumulation with increased fat content could be a major contributor to the decreased thermogenic potential of human BAT.

In this study, CPF only increased weight gain when combined with a high-fat diet. On one hand, the high amount of fat in the diet stimulated the absorption of lipophilic molecules [86]. On the other hand, the accumulation of CPF in adipocytes also promoted lipid accumulation by inhibiting thermogenic activity and disrupting lipogenic/lipolytic balances. Such HFD-dependent effect suggests that in certain populations, especially those who mostly consume a western or keto diet, CPF may be more detrimental to their health. This is coupled with metabolic pressures brought on by high-fat food themselves.

AMPK is an intracellular energy sensor that regulates brown adipocyte development and metabolism [87]. It is required for maintaining mitochondrial integrity

and maintain mitochondrial homeostasis by promoting autophagy/mitophagy. A previous study has also shown that the deletion of AMPK in adipocytes leads to reductions in mitochondrial function and content [60]. Experimental results found that CPF hindered the mitophagy activation and reduced thermogenic capacity of BAT, which is similar to what was found in AMPK knockout mice [60], pointing to the importance of AMPK in the context of dietary CPF exposure.

Like all experiments our studies had several limitations. Firstly, food intake was modestly increased in mice fed a high-fat diet and treated with CPF. This increase in food intake, in combination with the reduction in BAT metabolic activity, may have contributed to the increased adiposity and metabolic dysfunction to some extent. Future studies are needed to investigate the effects of CPF in high-fat diet fed mice that have similar caloric intake.

Secondly, the actual level of CPF in circulation could not be determined during the experiment. The traditional method to determine circulating CPF levels are to measure 3,5,6-trichlorpyridinol (TCPy) in the urine. This is because CPF is first converted to chlorpyrifos-oxon before being metabolized to TCPy and then excreted in urine. Most studies have utilized TCPy as a biomarker of exposure to CPF, on the assumption that CPF is the only source of TCPy in urine and that 70% of the absorbed dose is converted to TCPy and eliminated in the urine [26]. However, this method is not accurate because TCPy is also a metabolite of other chemicals. For example, in NHANES III study [26], the CPF intake measured directly in food was estimated to be 0.46 µg/day on average, but the amount of TCPy excreted in urine averaged 6.3 µg/day.

Besides, TCPy itself also exists in food which contributes directly to urinary TCPy. For these reasons, TCPy was not a great indicator for monitoring CPF. In addition, we did not have access the amount of circulating CPF level in the serum. Though we aimed for a dosage of 0.5mg/kg/BW for low dose and 2 mg/kg BW for high dose exposures respectively, the actual amount circulating in the body was unknown. In the future, gas chromatography/mass spectrometry (GC/MS) may be a potential tool to measure the circulating CPF level in serum.

Lastly, only C57BL6J male mice were used in this study. Due to hormonal changes brought about by the menstrual cycle in female mice, metabolism studies in female mice were not conducted. In addition, many previous studies have shown that male mice are more prone to obesity [88] -. Moreover, a further study by Slotkin et al. [89] showed that developmental exposure to CPF elicits sex-selective hyperlipidemia and hyperinsulinemia; concluding that other metabolic parameters and BAT function may also be affected by CPF differently. As some hormonal regulations are sex-dependent, studies using a female mouse model is necessary to elucidate the effect of both CPF on BAT in females and its potential metabolic implications.

Future Directions:

To determine if the effect of CPF on metabolism is mediated through reductions in adipose tissue AMPK, mice lacking adipose tissue specific expression of AMPK [60] could be fed a high-fat diet with CPF. Additionally, specific AMPK activators such as MK8722 [90] or compound 991 [91] could be combined with CPF, to determine if they

can negate the effect of CPF in vivo. Furthermore, the anti-diabetic drug metformin has been shown to activate AMPK [92], as well as salicylate [93]. Therefore, such compounds, having been proven safe for humans, may be potential treatments to combat obesity caused by CPF exposure.

To test CPF's potential to affect human BAT function and mitochondria damage, it would be interesting to conduct a clinical study on people with occupational exposure, measuring their BAT metabolic activity using MRI. *In vitro* experiments could also be done using human brown adipocytes. Testing the effects of other widely-used pesticides and chemicals on BAT activity would also be worthwhile.

Currently, CPF is banned for residential use but not for agricultural applications. As one of the mostly-used pesticides in the world, CPF has contributed greatly to agricultural production. However, the prolonged damage for public's health and tremendous burden for the healthcare system may be enough to negate the economic benefits, given the obesity epidemic.

Chapter VI: CONCLUSIONS

This thesis examines the effect of chlorpyrifos, an environmental toxin, on energy balance, glucose homeostasis, liver lipids and brown adipose tissue in mice. We exposed C57BL6/J mice to dietary CPF at two different doses, which mice can tolerate without any neuronal damage. We found that CPF treatment, in combination with a high-fat diet, induced excess accumulations of lipid in the body and reductions in energy expenditure, which are associated with impairments in mitochondrial morphology that may due to reduced AMPK and mitophagy.

These findings suggest that long-term exposure to CPF, when consumed with a high-fat diet, could cause increased obesity and metabolic dysfunction. Certain populations, such as farmers who are occupationally exposed, need special attention regarding their long-term health and safety. Further research is required to delineate the molecular mechanisms of CPF's detrimental effects and potential treatments to mitigate such damage brought on by this environmental toxin.

REFERENCES

[1] K. Naser, A. Gruber and G. Thomson, "The emerging pandemic of obesity and diabetes: are we doing enough to prevent a disaster?," International Journal of Clinical Practice, vol. 60, no. 9, pp. 1093-1097, 2006.

[2] World Health Organization, "Obesity and overwight," February 2018. [Online]. Available: https://www.who.int/news-room/fact-sheets/detail/obesity-and-overweight.

[3] J. R. Koethe et al., "Rising Obesity Prevalence and Weight Gain Among Adults Starting Antiretroviral Therapy in the United States and Canada," AIDS Research and Human Retroviruses, pp. 50-58, 2016.

[4] D.P. Rao et al., "Childhood overweight and obesity trends in Canada,". Health Promot Chronic Dis Prev Can., vol. 36, no.9, pp.194–198, 2016.

[5] A. Ershow, "Environmental influences on development of type 2 diabetes and obesity: challenges in personalizing prevention and management," Journal of Diabetes Science and Technology, vol. 3, no. 4, pp. 727-734, 2009.

[6] P. Poirier et al., "Obesity and cardiovascular disease: pathophysiology, evaluation, and effect of weight loss: an update of the 1997 American Heart Association Scientific Statement on Obesity and Heart Disease from the Obesity Committee of the Council on Nutrition, Physical," Circulation, vol. 113, no. 6, pp. 898-918, 2006.

[7] M. Benedict and X. Zhang, "Non-alcoholic fatty liver disease: An expanded review," World Journal of Hepatology, vol. 9, no. 16, pp. 715-732, 2017.

[8] M. Kasuga, "Insulin resistance and pancreatic beta cell failure," Journal of Clinical Investigation, vol. 116, no. 7, pp. 1756-1760, 2006.

[9] A.S. Al-Goblan et al., "Mechanism linking diabetes mellitus and obesity," Diabetes Metab Syndr Obes, vol. 7, pp.587-591, 2014.

[10] P. Poirier and R. Eckel, "Obesity and cardiovascular disease," Current Atheroschlerosis Reports, vol. 4, no. 6, pp. 448-453, 2002.

[11] J. Temple, P. Cordero, V. Nguyen and J. Oben, "A Guide to Non-Alcoholic Fatty Liver Disease in Childhood and Adolescence," Int J Mol Sci. vol. 17, no. 6, 2016.

[12] M. Goran, G. Ball and M. Cruz, "Obesity and Risk of Type 2 Diabetes and Cardiovascular Disease in Children and Adolescents," The Journal of Clinical Endocrinology & Metabolism, vol. 88, no. 4, pp. 1417-1427, 2013.

[13] Obesity Canada, "Obesity In Canada," March 2019. [Online]. Available: https://obesitycanada.ca/obesity-in-canada/.

[14] G. Doucet and M. Beatty, "The Cost of Diabetes in Canada: The Economic Tsunami," Canadian Journal of Diabetes, vol. 34, no. 1, pp. 27-29, 2010.

[15] P. Baillie-Hamilton, "Chemical toxins: a hypothesis to explain the global obesity epidemic," Journal of Alternative and Complementary Medicine, vol. 8, no. 2, pp. 185-192, 2002.

[16] K. Singh and H. Chan, "Persistent organic pollutants and diabetes among Inuit in the Canadian Arctic," Environment International, vol. 101, pp. 183-189, 2017.

[17] C. Kassotics and H. Stapleton, "Endocrine-Mediated Mechanisms of Metabolic Disruption and New Approaches to Examine the Public Health Threat," Frontiers in Endocrinology, vol. 10, p. 39, 2019.

[18] I. D. Gregorio et al. , "Environmental Pollutants Effect on Brown Adipose Tissue," Foundation Physiotherapy, p. 1891, 2019.

[19] J. Arrebola et al., "Relationship between serum concentrations of persistent organic pollutants and markers of insulin resistance in a cohort of women with a history of gestational diabetes mellitus," Environmental Research, vol. 136, pp. 435-440, 2016.

[20] G. Howell, C. Mulligan and J. Chambers, "Effect of chronic p,p'-dichlorodiphenyldichloroethylene (DDE) exposure on high fat diet-induced alterations in glucose and lipid metabolism in male C57BL/6H mice," Toxicology, vol. 328, pp. 112-22, 2015.

[21] J. Arrebola et al., "Adipose tissue concentrations of persistent organic pollutants and prevalence of type 2 diabetes in adults from Southern Spain," Environmental Research, vol. 122, pp. 31-37, 2013.

[22] J. Suarez-Lopez et al., "Persistent organic pollutants in young adults and changes in glucose related metabolism over a 23-year follow-up," Environmental Research, vol. 137, pp. 485-494, 2015.

[23] M. Montgomery et al. , "Incident diabetes and pesticide exposure among licensed pesticide applicators: Agricultural Health Study, 1993-2003," American Journal of Epidemiology, vol. 167, no. 10, pp. 1235-1246, 2008.

[24] T. Saldana et al., "Pesticide exposure and self-reported gestational diabetes mellitus in the Agricultural Health Study," Diabetes Care, vol. 30, no. 3, pp. 529-534, 2007.

[25] S. Mansour and L. Gamet-Payrastre, "Ameliorative effect of vitamin E to mouse dams and their pups following exposure of mothers to chlorpyrifos during gestation and lactation periods," Toxicology and Industrial Health, vol. 32, no. 7, pp. 1178-1196, 2016.

[26] D. L. Eaton et al., "Review of the toxicology of chlorpyrifos with an emphasis on human exposure and neurodevelopment," Critical Reviews in Toxicology, vol. 38, no. 1, pp. 1-125, 2008.

[27] C. Timchalk et al., "A Physiologically Based Pharmacokinetic and Pharmacodynamic (PBPK/PD) Model for the Organophosphate Insecticide Chlorpyrifos in Rats and Humans," Toxicological Sciences, vol. 66, no. 1, pp. 34-53, 2002.

[28] D. Barr and J. Angerer, "Potential uses of biomonitoring data: a case study using the organophosphorus pesticides chlorpyrifos and malathion," Environmental Health Perspectives, vol. 114, no. 11, pp. 1763-1769, 2006.

[29] United States Environmental Protection Agency, "Chlorpyrifos," March 2019. [Online]. Available: https://www.epa.gov/ingredients-used-pesticide-products/chlorpyrifos.

[30] T. Lassiter and S. Brimijoin, "Rats gain excess weight after developmental exposure to the organophosphorothionate pesticide, chlorpyrifos," Neurotoxicology

Teratology, vol. 30, no. 2, pp. 125-130, 2008.

[31] S. Kondakela, J. Lee, M. Ross and G. Howell, "Effects of acute exposure to chlorpyrifos on cholinergic and non-cholinergic targets in normal and high-fat fed male C57BL/6J mice," Toxicology and Applied Pharmacology, vol. 337, pp. 65-75, 2017.

[32] Liang, Y., et al., "Organophosphorus pesticide chlorpyrifos intake promotes obesity and insulin resistance through impacting gut and gut microbiota," Microbiome, vol. 7, no.1, pp.19, 2019.

[33] J. Heindel, "History of the Obesogen Field: Looking Back to Look Forward," Frontiers in Endocrinology, vol. 10, p. 14, 2019.

[34] B. Cannon and J. Nedergaard, "Brown adipose tissue: function and physiological significance," Physiological Reviews, vol. 84, no. 1, pp. 277-359, 2004.

[35] E. Rosen and B. Spiegelman, "What we talk about when we talk about fat," Cell, vol. 156, no. 1-2, pp. 20-44, 2014.

[36] J. Wu et al., "Beige adipocytes are a distinct type of thermogenic fat cell in mouse and human," Cell, vol. 150, no. 2, pp. 366-376, 2012.

[37] W. v. M. Lichtenbelt, "Brown adipose tissue and the regulation of nonshivering thermogenesis," Current Opinion in Clinical Nutrition & Metabolic Care, vol. 15, no. 6, pp. 547-552, 2012.

[38] J. Nedergaard et al., "Unexpected evidence for active brown adipose tissue in adult

humans," American Journal of Physiology Endocrinology and Metabolism, vol.293, pp.444-452, 2007.

[39] M. Saito et al., "High incidence of metabolically active brown adipose tissue in healthy adult humans: effects of cold exposure and adiposity," Diabetes, vol. 58, no. 7, pp. 1526-1531, 2009.

[40] A. Cypess et al., "Identification and importance of brown adipose tissue in adult humans," The New England Journal of Medicine, vol. 360, no. 15, pp. 1509-1517, 2009.

[41] W. v. M. Lichtenbelt et al., "Cold-activated brown adipose tissue in healthy men," The New England Journal of Medicine, vol. 360, no. 15, pp. 1500-1508, 2009.

[42] K. Virtanen et al., "Functional brown adipose tissue in healthy adults," The New England Journal of Medicine, vol. 360, no. 15, pp. 1518-1525, 2009.

[43] V. Ouellet et al., "Outdoor temperature, age, sex, body mass index, and diabetic status determine the prevalence, mass, and glucose-uptake activity of 18F-FDG-detected BAT in humans," The Journal of Clinical Endocrinology and Metabolism, vol. 96, no. 1, pp. 192-199, 2011.

[44] Crane, J.D., et al., "A standardized infrared imaging technique that specifically detects UCP1-mediated thermogenesis in vivo," Mol Metab, vol. 3, no. 4, pp. 490-4, 2014.

[45] Feldmann, H.M., et al., "UCP1 ablation induces obesity and abolishes diet-induced thermogenesis in mice exempt from thermal stress by living at thermoneutrality,"

Cell metabolism, vol.9, no. 2, pp.203-209, 2009.

[46] A. Pfeifer and L. Hoffman, "Brown, beige, and white: the new color code of fat and its pharmacological implications," Annual Review of Pharmacology and Toxicology, vol. 55, pp. 207-227, 2015.

[47] V. Peirce, S. Carobbio and A. Vidal-Puig, "The different shades of fat," Nature, vol. 510, no. 7503, pp. 76-83, 2014.

[48] K. Townsend and Y. Tseng, "Brown fat fuel utilization and thermogenesis," Trends in Endocrinology & Metabolism, vol. 25, no. 4, pp. 168-177, 2014.

[49] Nicholls, D. G. & Rial, E. A, "History of the First Uncoupling Protein, UCP1," J. Bioenerg. Biomembr, vol.31, pp.399-406, 1999.

[50] A. Cypess et al., "Activation of human brown adipose tissue by a β3-adrenergic receptor agonist," Cell Metabolism, vol. 21, no. 1, pp. 33-38, 2015.

[51] F. Villarroya, R. Cereijo, J. Villarroya and M. Giralt, "Brown adipose tissue as a secretory organ," Nature Reviews Endocrinology, vol. 13, no. 1, pp. 26-35, 2017.

[52] D. C. Wallace, "A Mitochondrial Paradigm of Metabolic and Degenerative Diseases, Aging, and Cancer: A Dawn for Evolutionary Medicine," Annual Review of Genetics, vol. 39, p. 359, 2005.

[53] S. Altshuler-Keylin and S. Kajimura, "Mitochondrial homeostasis in adipose tissue remodeling," Science Signaling, vol. 10, no. 468, 2017.

[54] W. Ding and X. Yin, "Mitophagy: mechanisms, pathophysiological roles, and

analysis," Biological Chemistry, vol. 393, no. 7, pp. 547-564, 2012.

[55] D. Egan et al., "Phosphorylation of ULK1 (hATG1) by AMP-activated protein kinase connects energy sensing to mitophagy," Science, vol.331, no.6016, pp.456-61, 2011.

[56] I. Kim, S. Rodriguez-Enriquez and J. Lemasters, "Selective degradation of mitochondria by mitophagy," Archives of Biochemistry and Biophysics, vol. 462, no. 2, pp. 245-253, 2007.

[57] P. Wong, C. Puente, I. Ganley and X. Jiang, "The ULK1 complex: sensing nutrient signals for autophagy activation," Autophagy, vol. 9, no. 2, pp. 124-137, 2013.

[58] J. Füllgrabe, D. Klionsky and B. Joseph, "The return of the nucleus: transcriptional and epigenetic control of autophagy," Nature Reviews Molecular Cell Biology, vol. 15, no. 1, pp. 65-74, 2014.

[59] D. Hardie, F. Ross and S. Hawley, "AMPK: a nutrient and energy sensor that maintains energy homeostasis," Nature Reviews Molecular Cell Biology, vol. 13, no. 4, pp. 251-262, 2012.

[60] E. Mottillo et al., "Lack of Adipocyte AMPK Exacerbates Insulin Resistance and Hepatic Steatosis through Brown and Beige Adipose Tissue Function," Cell Metabolism, vol. 24, no. 1, pp. 118-129, 2016.

[61] Moellering, D.R. and D.L. Smith, Jr., "Ambient Temperature and Obesity," Curr Obes Rep, vol.1, no.1, pp. 26-34, 2012.

[62] Fischer, A.W., B. Cannon, and J. Nedergaard, "Optimal housing temperatures forvmice to mimic the thermal environment of humans: An experimental study," Mol Metab, vol. 7, pp. 161-170, 2018.

[63] Riederer, A.M., et al., "Pyrethroid and organophosphorus pesticides in composite diet samples from Atlanta, USA adults," Environ Sci Technol, vol. 44, no.1, pp. 483-90, 2010.

[64] Huff, R.A., A.W. Abu-Qare, and M.B. Abou-Donia, "Effects of sub-chronic in vivo chlorpyrifos exposure on muscarinic receptors and adenylate cyclase of rat striatum," Arch Toxicol, vol. 75, no.8, pp. 480-6, 2011.

[65] Mehlem, A., et al., "Imaging of neutral lipids by oil red O for analyzing the metabolic status in health and disease," Nat Protoc, vol. 8, no.6, pp. 1149-54, 2013.

[66] A. Poole et al., "The PINK1/Parkin pathway regulates mitochondrial morphology," Proceedings of the National Academy of Sciences of the United States of America, vol. 105, no. 5, pp. 1638-1643, 2008.

[67] J. D. Crane, et al., "A standardized infrared imaging technique that specifically detects UCP1-mediated thermogenesis in vivo," Mol. Metab. vol. 3, pp.490–494, 2014.

[68] Liu, J., et al., "Free fatty acids, not triglycerides, are associated with non-alcoholic liver injury progression in high fat diet induced obese rats," Lipids in health and disease, vol15, no. 1, pp. 27, 2016.

[69] X. Xiong et al., "Obeticholic acid protects mice against lipopolysaccharide-induced liver injury and inflammation," Biomedicine & Pharmacotherapy, vol. 96, pp. 1292-1298, 2017.

[70] Peris-Sampedro, Fiona, et al. "Adulthood Dietary Exposure to a Common Pesticide Leads to an Obese-Like Phenotype and a Diabetic Profile in apoE3 Mice." Environmental research, vol. 142, pp. 169-76, 2015.

[71] F. Peris-Sampedro et al., "Chronic exposure to chlorpyrifos triggered body weight increase and memory impairment depending on human apoE polymorphisms in a targeted replacement mouse model," Physiology and Behavior, vol. 144, pp. 37-45, 2015.

[72] Vijgen, Guy H E J et al. "Brown adipose tissue in morbidly obese subjects." PloS one vol. 6, no. 2, 2011.

[73] Altshuler-Keylin, S. and S. Kajimura, "Mitochondrial homeostasis in adipose tissue remodeling," Sci Signal, vol. 10, no. 467, 2017.

[74] Liu, W.J, et al., "p62 links the autophagy pathway and the ubiqutin-proteasome system upon ubiquitinated protein degradation," Cell Mol Biol Lett, vol. 21, pp. 29, 2016.

[75] S. Stein et al., "The regulation of AMP-activated protein kinase by phosphorylation," Biochemical Journal, vol. 345, pp. 437-443, 2000.

[76] J. Ha et al., "Critical phosphorylation sites for acetyl-CoA carboxylase activity,"

Journal of Biological Chemistry, vol. 269, no. 35, pp. 22162-22168, 1994.

[77] E. Jackson et al., "Adipose Tissue as a Site of Toxin Accumulation,"
Comprehensive Physiology, vol. 7, no. 4, pp. 1085-1135, 2017.

[78] E. Tanvir et al., "A model of chlorpyrifos distribution and its biochemical effects on
the liver and kidneys of rats," Human & Experimental Toxicology, vol. 35, no. 9,
pp. 991-1004, 2016.

[79] R. Huff, A. Abu-Qare and M. Abou-Donia, "Effects of sub-chronic in vivo
chlorpyrifos exposure on muscarinic receptors and adenylate cyclase of rat
striatum," Archives of Toxicology, vol. 75, no. 8, pp. 480-486, 2001.

[80] N. Akhtar, M. Srivastava and R. Raizada, "Assessment of chlorpyrifos toxicity
on certain organs in rat, Rattus norvegicusv," Journal of Environmental
Biology, vol. 30, no. 6, pp. 1047-1053, 2009.

[81] W. Meggs and K. Brewer, "Weight gain associated with chronic exposure to
chlorpyrifos in rats," Journal of Medical Toxicology, vol. 3, no. 3, pp. 89-93,
2007.

[82] B. Fang et al., "Chronic chlorpyrifos exposure elicits diet-specific effects on
metabolism and the gut microbiome in rats," Food and Chemical Toxicology,
vol. 111, pp. 144-152, 2018.

[83] A. Bartelt and J. Heeren, "Adipose tissue browning and metabolic health,"
Nature Reviews Endocrinology, vol. 10, no. 1, pp. 24-36, 2014.

[84]   S. Wijers, W. Saris and W. v. M. Lichtenbelt, "Cold-induced adaptive thermogenesis in lean and obese," Obesity, vol. 18, no. 6, pp. 1092-1099, 2010.

[85]   T. Yoneshiro et al., "Age-related decrease in cold-activated brown adipose tissue and accumulation of body fat in healthy humans," Obesity, vol. 19, no. 9, pp. 1755-1760, 2011.

[86]   C. Porter, N. Trevaskis and W. Charman, "Lipids and lipid-based formulations: optimizing the oral delivery of lipophilic drugs," Nature Reviews Drug Discovery, vol. 6, no. 3, pp. 231-248, 2007.

[87]   E. Desjardins and G. Steinberg, "Emerging Role of AMPK in Brown and Beige Adipose Tissue (BAT): Implications for Obesity, Insulin Resistance, and Type 2 Diabetes," Current Diabetes Reports, vol. 18, no. 10, p. 80, 2018.

[88]   Y. Yang et al., "Variations in body weight, food intake and body composition after long-term high-fat diet feeding in C57BL/6J mice," Obesity (Silver Spring, Md.,) vol. 22, no. 10, 2014.

[89]   B. Slotkin et al., "Developmental Exposure of Rats to Chlorpyrifos Elicits Sex-Selective Hyperlipidemia and Hyperinsulinemia in Adulthood." Environmental Health Perspectives, vol. 113, no.10, pp. 1291-1294, 2005.

[90] R. Myers et al., "Systemic pan-AMPK activator MK-8722 improves glucose homeostasis but induces cardiac hypertrophy," Science, vol. 357, no. 6350, pp. 507-511, 2017.

[91] L. Bultot et al., "Benzimidazole derivative small-molecule 991 enhances AMPK activity and glucose uptake induced by AICAR or contraction in skeletal muscle," American Journal of Physiology-Endocrinology and Metabolism, vol. 311, no. 4, pp. E706-E719, 2016.

[92] G. Zhou et al., "Role of AMP-activated protein kinase in mechanism of metformin action," Journal of Clinical Investigation, vol. 108, no. 8, pp. 1167-1174, 2001.

[93] S. Hawley et al., "The ancient drug salicylate directly activates AMP-activated protein kinase," Science, vol. 336, no. 6083, pp. 918-922, 2012.

[94] B. Dannenmann et al., "Simultaneous quantification of DNA damage and mitochondrial copy number by long-run DNA-damage quantification (LORD-Q)," Oncotarget, vol. 8, no. 68, pp. 112417-112425, 2017.

[95] H. Feldmann et al., "UCP1 ablation induces obesity and abolishes diet-induced thermogenesis in mice exempt from thermal stress by living at thermoneutrality," Cell Metabolism, vol. 9, pp. 203-209, 2009.

[96] V. Golozoubova et al., "Depressed thermogenesis but competent brown adipose tissue recruitment in mice devoid of all thyroid hormone receptors," Molecular Endocrinoligy, vol.18, pp. 384-401, 2004.

[97] L.Kozak & R. Anunciado-Koza, "UCP1: its involvement and utility in obersity," Intvernational Journal of Obesity, vol.32, pp.32-38, 2008.